The Effect of Surface Tectonic Plates and Lateral Viscosity Variations on Global Mantle Flow Models in Spherical Geometry

Alessandro Forte

フォルテ　　　　　アレックス

強　　　荒楠

Proposed (Tentative!) Outline of Lecture

1. **Introduction**
   ●

2. **Analytic Spectral Description of Surface Plate Kinematics**
   ●

3. **Dynamical Models of Rigid Plate Motions Coupled to Mantle Flow**

   ●

4. **Quasi-analytic Modelling of Mantle Flow with Lateral Viscosity Variations**

   ●

1. Introduction

1.1. Sub-solidus flow and effective mantle viscosity

The ability of the mantle to creep or 'flow' over geological time scales is due to the presence of natural *imperfections* in the crystalline structure of the minerals which constitute the rocks in the mantle. These imperfections are actually atomic-scale *defects* in the lattice of the crystal grains in minerals (*e.g., Nicolas & Poirier*, 1976; *Carter*, 1976; *Weertman*, 1978). If the ambient temperature is sufficiently high, the imposition of stresses on the rocks will cause the mineral defects to propagate and they thus permit mantle rocks to effectively 'flow'. The flow can persist for as long as the imposed stresses are maintained and thus mantle deformation can achieve a steady state rate.

The steady-state creep of mantle rocks may then be characterized by a single parameter called the *effective viscosity* (*e.g., Gordon*, 1965; *Weertman & Weertman*, 1975). A general formula for the effective viscosity of the mantle, which is based on the microphysical creep mechanisms described in the references cited above,

is as follows:

$$\eta = A \, d^m \, \tau^{-n} \, \mathrm{k}T \, \exp\left[\frac{\Delta E + P\Delta V}{\mathrm{k}T}\right] \tag{1}$$

in which A is a dimensional constant which depends on the details of the creep processes, d is the effective *grain size* of the crystal grains, $\tau = \sqrt{\tau_{ij}\tau_{ij}}$ is the square root of the second invariant of the *deviatoric stress* field (*Stocker & Ashby, 1973*), k is Boltzmann's constant, T is the *absolute temperature*, ΔE is the creep *activation energy*, ΔV is the creep *activation volume*, and P is the total ambient *pressure*.

If mantle creep occurs primarily through the *diffusion* of point defects, the effective viscosity in expression (1) is independent of stress (*i.e.*, $n = 0$). For this *diffusion creep* the dependence on grain size is significant and generally m ranges from 2 to 3. An alternative mechanism for mantle creep involves the glide and climb of *dislocations*, in which case the effective viscosity in (1) will be independent of grain size (*i.e.*, $m = 0$) but will be sensitive to ambient deviatoric stress. For this *dislocation creep*, laboratory experiments on olivine or dunite suggest the stress exponent n will be near 3 (*e.g.*, *Post & Griggs, 1973*).

The theoretical expression (1) does not explicitly show the importance of *chemical*

environment (*e.g.*, H_2O, CO_2) on mantle viscosity. Many studies have suggested a strong impact of chemistry on mantle creep (*e.g., Ricoult & Kohlstedt*, 1985; *Karato et al.* 1986; *Borch & Green*, 1987; *Hirth & Kohlstedt*, 2003).

The strong dependence of effective viscosity on temperature and pressure can be represented in terms of a *homologous temperature, T/T_{melt}*, as follows:

$$\eta = \eta_o \exp \left[g \frac{T_{melt}}{T} \right] \tag{2}$$

This dependence of viscosity on melting temperature, which has been observed in metallurgy, was extended to the crystalline rocks in the mantle by *Weertman* (1970) for the purpose of estimating viscosity in the deep mantle. The factor g in expression (2) is empirical, and is used to relate the activation enthalpy $\Delta E + P\Delta V$ in expression (1) to melting temperature:

$$\frac{\Delta E + P\Delta V}{k} = g \, T_{melt}$$

The utility of using expression (2) is that knowledge of the pressure-dependence of activation energy and activation volume, which is difficult to measure directly

at high pressures, can be replaced by pressure-dependent melting temperature. The latter can be measured at moderate pressures and extrapolated to high pressures (*i.e.,* the deep mantle). For olivine, g values between 20 and 30 have been suggested, depending on whether diffusion or dislocation creep are assumed (*e.g., Weertman & Weertman*, 1975).

The use of expression (2) may not be a valid approximation in the deep mantle, as suggested by previous debates on the interpretation of experimentally measured melting curves for the lower mantle (*e.g., Brown*, 1993). It is therefore possible that the empirical factor g in (2) may not be effectively constant, as assumed by (*Weertman & Weertman*, 1975) and others since.

The main conclusion we should extract from this brief discussion is that the dependence of effective viscosity on grain size or stress, on ambient temperature and pressure, and also on chemical environment, implies the viscosity in the mantle should be strongly heterogeneous. Such lateral heterogeneity appears to be especially important in the lithosphere, where the effectively rigid tectonic plates are bounded by ridges, trenches and transform faults where strong deformation is occurring. Similarly, the lateral temperature variations

maintained by the thermal convection process in the mantle should also give rise to corresponding lateral viscosity variations, owing to the strong temperature dependence evident in expressions (1-2).

In Lecture 1 we developed a mantle flow theory on the assumption that the dominant variation of viscosity is with depth. In this Lecture we will consider how we may extend the flow theory to account for the dynamical impact of lateral viscosity variations in the mantle.

1.2. Momentum conservation with 3-D viscosity heterogeneity

Let us first consider the most general expression of the governing hydrodynamic equations for an infinite Prandtl number fluid with an arbitrary 3-D variation of $\eta(r, \theta, \phi)$, dynamic viscosity coefficient.

Recall from Lecture 1 that the fluid-mechanical equation of momentum conservation, for an infinite Prandtl number fluid, is

$$\partial_j \sigma_{ij} + \rho_o \partial_i \phi_1 - \rho_1 \mathrm{g}_o \hat{\boldsymbol{r}} = 0 \tag{3}$$

in which

$$\sigma_{ij} = -P_1 \delta_{ij} + \eta \left(\partial_i u_j + \partial_j u_i - \frac{2}{3} \delta_{ij} \, \partial_k u_k \right) \tag{4}$$

In these equations we use the convenient notation ∂_i to represent partial differentiation $\partial/\partial x_j$ along the Cartesian coordinate direction x_i. It should be noted that in equation (3), we describe the dynamics relative to a hydrostatic reference configuration (identified by the subscript $_o$).

On the basis of the constitutive relation (4), we find that the divergence of the stress tensor $\partial_j \sigma_{ij}$, which is required in (3), is as follows:

$$\partial_j \sigma_{ij} = -\partial_i P_1 + \frac{1}{3} \eta \partial_i (\partial_k u_k) - \frac{2}{3} (\partial_i \eta)(\partial_k u_k) + \eta \partial_j \partial_j u_i$$
$$+ (\partial_j \eta)(\partial_j u_i) + \partial_i (u_j \partial_j \eta) - u_j \partial_j (\partial_i \eta) . \tag{5}$$

Employing vector notation, we may rewrite this last expression as:

$$\boldsymbol{\nabla} \cdot \boldsymbol{\sigma} = -\boldsymbol{\nabla} P_1 + \frac{1}{3}\eta\boldsymbol{\nabla}(\boldsymbol{\nabla} \cdot \mathbf{u}) - \frac{2}{3}(\boldsymbol{\nabla} \cdot \mathbf{u})\boldsymbol{\nabla}\eta + \eta\nabla^2\mathbf{u}$$
$$+(\boldsymbol{\nabla}\eta \cdot \boldsymbol{\nabla})\mathbf{u} + \boldsymbol{\nabla}(\mathbf{u} \cdot \boldsymbol{\nabla}\eta) - (\mathbf{u} \cdot \boldsymbol{\nabla})\boldsymbol{\nabla}\eta \,. \tag{6}$$

By virtue of the vector calculus identity

$$\boldsymbol{\nabla}(\mathbf{A} \cdot \mathbf{B}) = (\mathbf{A} \cdot \boldsymbol{\nabla})\mathbf{B} + (\mathbf{B} \cdot \boldsymbol{\nabla})\mathbf{A} + \mathbf{A} \times (\boldsymbol{\nabla} \times \mathbf{B}) + \mathbf{B} \times (\boldsymbol{\nabla} \times \mathbf{A}) \,,$$

we may rewrite expression (6) as:

$$\boldsymbol{\nabla} \cdot \boldsymbol{\sigma} = -\boldsymbol{\nabla} P_1 + \frac{1}{3}\eta\boldsymbol{\nabla}(\boldsymbol{\nabla} \cdot \mathbf{u}) - \frac{2}{3}(\boldsymbol{\nabla} \cdot \mathbf{u})\boldsymbol{\nabla}\eta + \eta\nabla^2\mathbf{u}$$
$$+2(\boldsymbol{\nabla}\eta \cdot \boldsymbol{\nabla})\mathbf{u} + \boldsymbol{\nabla}\eta \times (\boldsymbol{\nabla} \times \mathbf{u}) \,. \tag{7}$$

Substituting this last expression into the momentum conservation equation (3),

finally yields:

$$-\boldsymbol{\nabla} P_1 + \eta \nabla^2 \mathbf{u} + \frac{1}{3} \eta \boldsymbol{\nabla}(\boldsymbol{\nabla} \cdot \mathbf{u}) - \frac{2}{3}(\boldsymbol{\nabla} \cdot \mathbf{u})\boldsymbol{\nabla}\eta + 2(\boldsymbol{\nabla}\eta \cdot \boldsymbol{\nabla})\mathbf{u}$$
$$+\boldsymbol{\nabla}\eta \times (\boldsymbol{\nabla} \times \mathbf{u}) + \rho_o \boldsymbol{\nabla}\phi_1 - \rho_1 \mathrm{g}_o \hat{\boldsymbol{r}} = 0 \qquad (8)$$

The mathematical and/or numerical solution of this general expression for momentum conservation presents a major challenge. In this Lecture we shall consider two rather different approaches for modelling the dynamical impact of lateral viscosity variations in the mantle. The first approach involves a direct calculation of the effect of rigid surface plates on buoyancy induced mantle flow, which is modelled with depth-dependent viscosity below the plates. Here it is assumed that the plates are the most extreme manifestation of lateral variations of rheology in the Earth. The technique for incorporating the plates can effectively be reduced to a complex surface boundary condition. In the second half of this Lecture we will consider a direct, quasi-analytic solution of equation (8), using an elegant variational principle. This approach will allow us to investigate the impact of an arbitrary 3-D variation in viscosity on buoyancy induced mantle flow.

2. Analytic Spectral Description of Surface Plate Kinematics

2.1. Analytic description of plate divergence and vorticity for N rigid plates

Since the tectonic plates may be treated as effectively rigid bodies, we then know from *Euler's theorem* (*e.g., Goldstein*, 1980) that the surface velocity field $\mathbf{v}(\theta, \phi)$ of N plates may be represented in terms of the sum of the rigid-body rotations of each plate:

$$\mathbf{v}(\theta, \phi) = \sum_{i=1}^{N} H_i(\theta, \phi)\, \boldsymbol{\omega}^i \times \mathbf{r} \tag{9}$$

in which the *plate function* $H_i(\theta, \phi) = 1$ wherever plate i is located and $H_i(\theta, \phi) = 0$ elsewhere, $\boldsymbol{\omega}^i$ is the angular velocity vector of plate i, and $\mathbf{r}$ is the postion of any point on the Earth's surface.

By virtue of the trivial identity $\sum_i H_i(\theta, \phi) = 1$, we may rewrite expression (9) as:

$$\mathbf{v}(\theta, \phi) = \sum_{i=1}^{N-1} H_i(\theta, \phi)\, (\boldsymbol{\omega}^i - \boldsymbol{\omega}^N) \times \mathbf{r} \;+\; \boldsymbol{\omega}^N \times \mathbf{r} \tag{10}$$

The last term on the right-hand side of expression (10) represents a *net rotation of the lithosphere* with the angular velocity of plate N. Except for this net rotation, we note that the surface plate velocity field in entirely described by the *relative rotation* of each plate relative to plate N. For example, the *NUVEL-1* plate-motion model (*DeMets et al.*, 1990) is specified by arbitrarily choosing the Pacific plate as the Nth reference plate.

A useful mathematical representation for the relative rotation vector $\boldsymbol{\omega}^i - \boldsymbol{\omega}^N$ is given by

$$\boldsymbol{\omega}^i - \boldsymbol{\omega}^N = \boldsymbol{\nabla}\Omega^i \tag{11}$$

where

$$\Omega^i = x_1(\omega_1^i - \omega_1^N) + x_2(\omega_2^i - \omega_2^N) + x_3(\omega_3^i - \omega_3^N) \tag{12}$$

in which (x_1, x_2, x_3) are the Cartesian components of the position vector $\mathbf{r}$ and ω_j^i denotes the jth Cartesian component of the rotation rate $\boldsymbol{\omega}^i$. We may

similarly show that

$$\boldsymbol{\omega}^N = \boldsymbol{\nabla}\Omega^N \tag{13}$$

where

$$\Omega^N = x_1\omega_1^N + x_2\omega_2^N + x_3\omega_3^N \tag{14}$$

Substitution of expressions (11 & 13) into equation (10) yields:

$$\mathbf{v}(\theta, \phi) = -\sum_{i=1}^{N-1} H_i(\theta, \phi)\boldsymbol{\Lambda}\Omega^i - \boldsymbol{\Lambda}\Omega^N \tag{15}$$

in which $\boldsymbol{\Lambda} = \mathbf{r} \times \boldsymbol{\nabla}$ is the angular-momentum operator introduced in Lecture 1 [see also *Backus* (1958) for more details].

We may now use this last expression (15) to determine the horizontal divergence

$(\boldsymbol{\nabla}_H \cdot \mathbf{v})$ and radial vorticity $(\hat{\mathbf{r}} \cdot \boldsymbol{\nabla} \times \mathbf{v})$ of the plate velocity field:

$$\boldsymbol{\nabla}_H \cdot \mathbf{v} = -\frac{1}{a} \sum_{i=1}^{N-1} \boldsymbol{\nabla}_1 H_i \cdot \boldsymbol{\Lambda} \Omega^i \tag{16}$$

and

$$\hat{\mathbf{r}} \cdot \boldsymbol{\nabla} \times \mathbf{v} = \frac{1}{a} \boldsymbol{\Lambda} \cdot \mathbf{v} = -\frac{1}{a} \sum_{i=1}^{N-1} \left[\boldsymbol{\Lambda} H_i \cdot \boldsymbol{\Lambda} \Omega^i + H_i \Lambda^2 \Omega^i \right] - \frac{1}{a} \Lambda^2 \Omega^N \tag{17}$$

in which $r = a$ is the mean radius of Earth's solid surface, $\boldsymbol{\nabla}_1$ is the horizontal gradient on a sphere of unit radius, and $\Lambda^2 = \boldsymbol{\Lambda} \cdot \boldsymbol{\Lambda}$ is the horizontal Laplacian operator on a unit sphere.

On the basis of the general expressions for the horizontal gradients of ordinary

spherical harmonics, $Y_\ell^m(\theta, \phi)$, presented in *Edmonds* (1960), we can show that:

$$
\begin{aligned}
\mathbf{\Lambda} Y_\ell^m \quad &= \quad \imath \left[\frac{\hat{\mathbf{e}}_-}{\sqrt{2}} a_\ell^m Y_\ell^{m+1} + \hat{\mathbf{e}}_0 m Y_\ell^m - \frac{\hat{\mathbf{e}}_+}{\sqrt{2}} a_\ell^{-m} Y_\ell^{m-1} \right] \\
\mathbf{\nabla}_1 Y_\ell^m \quad &= \quad \frac{\hat{\mathbf{e}}_-}{\sqrt{2}} \left[\ell c_\ell^m Y_{\ell+1}^{m+1} + (\ell+1) c_{\ell-1}^{-m-1} Y_{\ell-1}^{m+1} \right] \\
&- \quad \hat{\mathbf{e}}_0 \left[\ell b_\ell^m Y_{\ell+1}^m - (\ell+1) b_{\ell-1}^m Y_{\ell-1}^m \right] \\
&+ \quad \frac{\hat{\mathbf{e}}_+}{\sqrt{2}} \left[\ell c_\ell^{-m} Y_{\ell+1}^{m-1} + (\ell+1) c_{\ell-1}^{m-1} Y_{\ell-1}^{m-1} \right]
\end{aligned}
\tag{18}
$$

in which we have

$$
a_\ell^m = [(\ell-m)(\ell+m+1)]^{1/2}, \quad b_\ell^m = \left[\frac{(\ell-m+1)(\ell+m+1)}{(2\ell+1)(2\ell+3)} \right]^{1/2}
$$
$$
c_\ell^m = \left[\frac{(\ell+m+2)(\ell+m+1)}{(2\ell+1)(2\ell+3)} \right]^{1/2}
\tag{19}
$$

and the complex basis vectors in (18) are defined as follows:

$$
\hat{\mathbf{e}}_+ = -\frac{1}{\sqrt{2}} \left(\hat{\mathbf{x}} + \imath \hat{\mathbf{y}} \right), \ \hat{\mathbf{e}}_0 = \hat{\mathbf{z}}, \ \hat{\mathbf{e}}_- = \frac{1}{\sqrt{2}} \left(\hat{\mathbf{x}} - \imath \hat{\mathbf{y}} \right)
\tag{20}
$$

where $\imath = \sqrt{-1}$, and $(\hat{\mathbf{x}}, \hat{\mathbf{y}}, \hat{\mathbf{z}})$ are the Cartesian unit basis vectors. Further details concerning the derivation of the expressions in (18) may be found in Appendix I

of *Forte & Peltier* (1994).

If we now expand the plate functions in term of spherical harmonics, as follows,

$$H_i(\theta, \phi) = \sum_{\ell=0}^{\infty} \sum_{m=-\ell}^{+\ell} (H_i)_\ell^m Y_\ell^m (\theta, \phi) \tag{21}$$

and then substitute (21) into (16-17), we can then use (18) to arrive at the following expressions for the harmonic coefficients of the plate divergence and vorticity:

$$(\boldsymbol{\nabla}_H \cdot \mathbf{v})_\ell^m = \sum_{i=1}^{N-1} \sum_{j=1}^{3} \left(S_j^i\right)_\ell^m \left(\omega_j^i - \omega_j^N\right) \tag{22}$$

$$(\hat{\mathbf{r}} \cdot \boldsymbol{\nabla} \times \mathbf{v})_\ell^m = \sum_{i=1}^{N-1} \sum_{j=1}^{3} \left(R_j^i\right)_\ell^m \left(\omega_j^i - \omega_j^N\right) + \sum_{j=1}^{3} \delta_{\ell 1} T_j^m \omega_j^N \tag{23}$$

in which the terms $\left(S_j^i\right)_\ell^m$ and $\left(R_j^i\right)_\ell^m$ are *linear functions* of the plate geometry

coefficients $(H_i)_\ell^m$. As shown in detail in Appendix III of *Forte & Peltier* (1994),

$$\left(S_j^i\right)_\ell^m \equiv S_j \left\{ (H_i)_{\ell+2}^m , (H_i)_\ell^m , (H_i)_{\ell-2}^m \right\} \tag{24}$$

$$\left(R_j^i\right)_\ell^m \equiv R_j \left\{ (H_i)_{\ell+1}^m , (H_i)_{\ell-1}^m \right\} \tag{25}$$

(24-25) show that the divergence and vorticity fields provide an *independent, complementary* sampling of the tectonic plate geometries. The degree ℓ *divergence* coefficients depend only on the degree $\ell + 2, \ell, \ell - 2$ plate geometry. The degree ℓ *vorticity* coefficients depend only on the degree $\ell + 1, \ell - 1$ plate coefficients.

2.2. Application to a hypothetical two-plate planet

We will now illustrate the use of the analytic expressions (22-23) by considering the following hypothetical planet with two hemispherical tectonic plates:
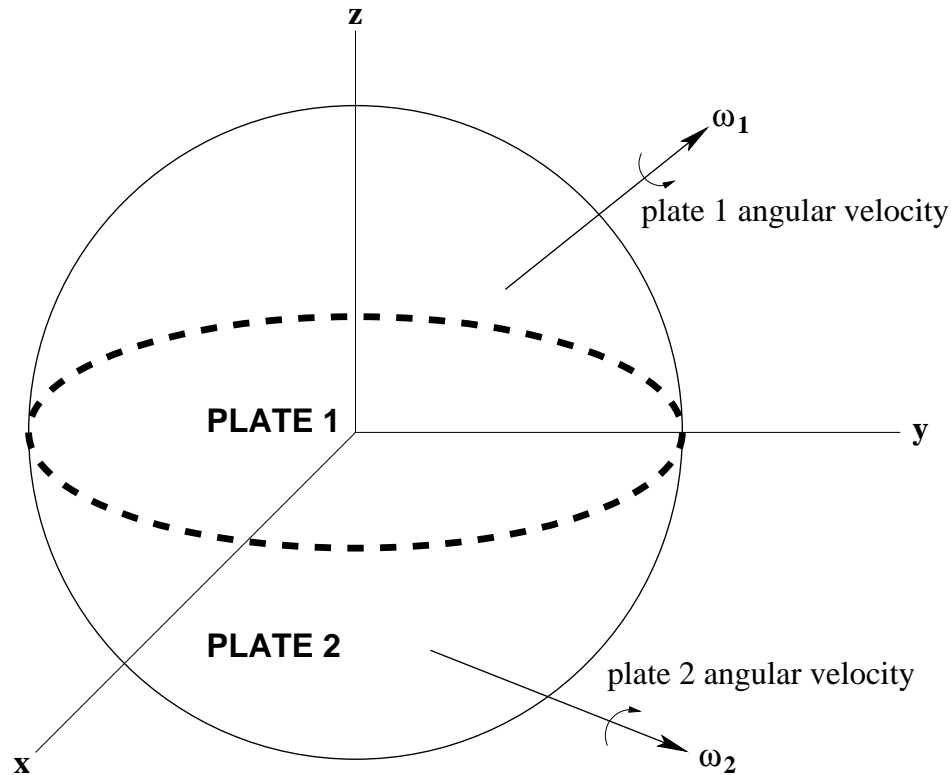
Fig. 1. Hypothetical planet with two hemispherical tectonic plates

If we assume that the plate boundary coincides with the equatorial plane of the planet we know that the *even degree coefficients* of each plate geometry function will vanish [*i.e.*, $(H_i)_\ell^m = 0$ for $\ell = 0, 2, 4...$]. This will also be true for any other orientation of the great-circle boundary between the two plates, since an arbitrary rotation of the coordinate system will not change the spectral

amplitudes of the plate functions (*e.g., Edmonds*, 1960). If we assume an equatorial plate boundary, we can derive the following expressions for the harmonic coefficients of the plate functions:

$$
\begin{aligned}
(H_1)_\ell^m &= \delta_{m0} \left[\tfrac{1}{2}\delta_{\ell 0} + \frac{P_{\ell-1}^m(0)}{\ell+1} \sqrt{\frac{2\ell+1}{2\ell-1}} \, (1 - \delta_{\ell 0}) \right] \\
(H_2)_\ell^m &= \delta_{m0} \left[\tfrac{1}{2}\delta_{\ell 0} - \frac{P_{\ell-1}^m(0)}{\ell+1} \sqrt{\frac{2\ell+1}{2\ell-1}} \, (1 - \delta_{\ell 0}) \right]
\end{aligned}
\tag{26}
$$

in which $P_\ell^m(x)$ is an associated Legendre polynomial which is normalized so that its root-mean-square amplitude is unity. We will assign the following, *arbitrarily chosen*, angular velocity vectors to the hemispherical plates:

$$
\omega_1 = \Omega\hat{\mathbf{z}} \,, \; \omega_2 = -\Omega \left(\frac{1}{2}\hat{\mathbf{x}} + \frac{\sqrt{3}}{2}\hat{\mathbf{z}} \right) \,, \; \Omega = 1°/Ma
\tag{27}
$$

Expression (26) shows that the amplitude spectrum of the hemispherical plate functions should decrease as $1/\ell$ with increasing degree. In contrast, since the plate divergence and vorticity fields involve gradients of the plate functions (see eqs. 16-17), which is equivalent to multiplying by ℓ in the spectral domain, we

expect the divergence and vorticity fields to have a flat amplitude spectrum. These expectations are confirmed in the figure below:
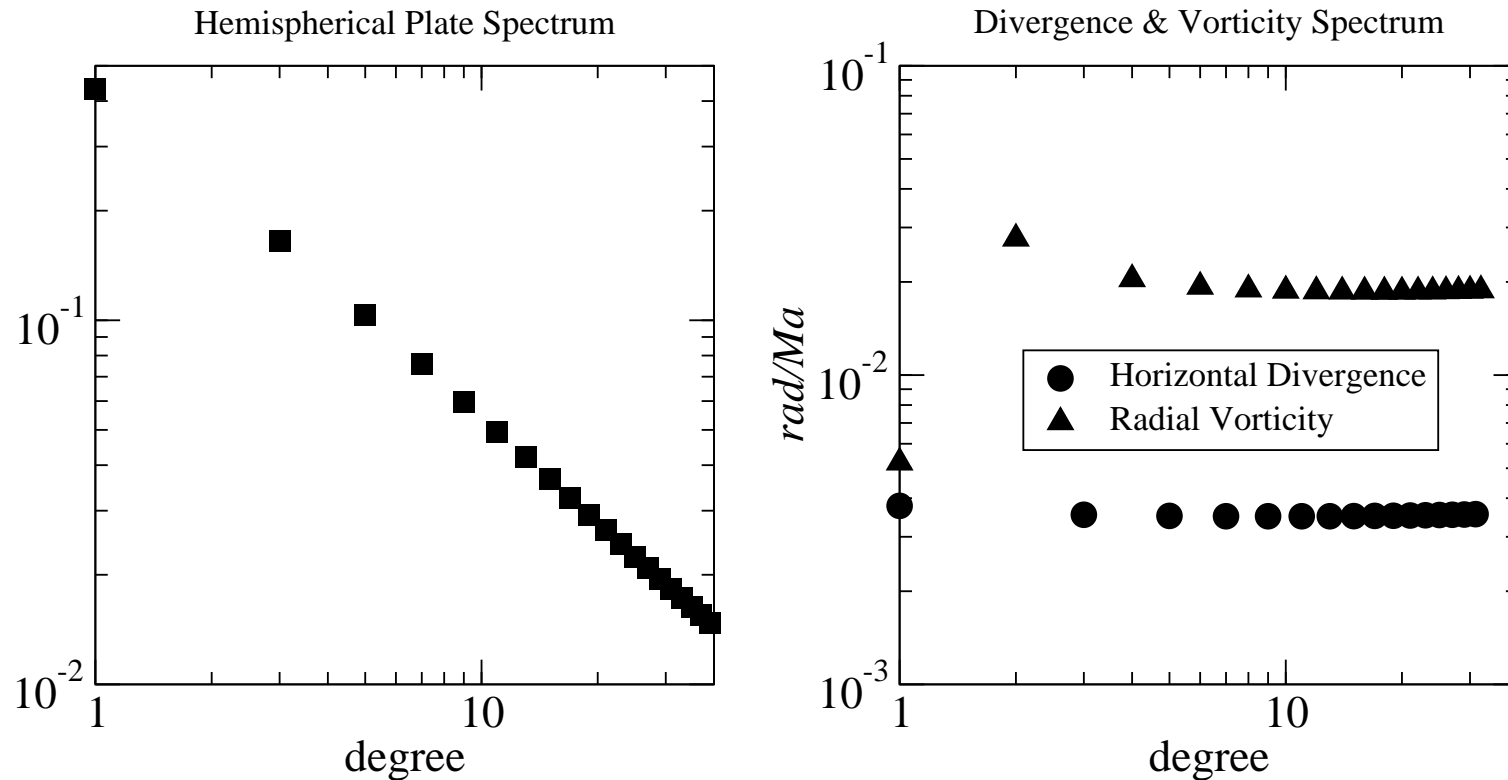

Fig. 2. Spectral amplitudes of hemispherical plate and corresponding divergence and vorticity.

The divergence and vorticity spectra shown above (Fig. 2) were calculated by substituting the plate coefficients (26) into expressions (22-23), using the rotation vectors in (27). In the maps below we show the predicted divergence and

vorticity fields resulting from the rotations of the two hemispherical plates.
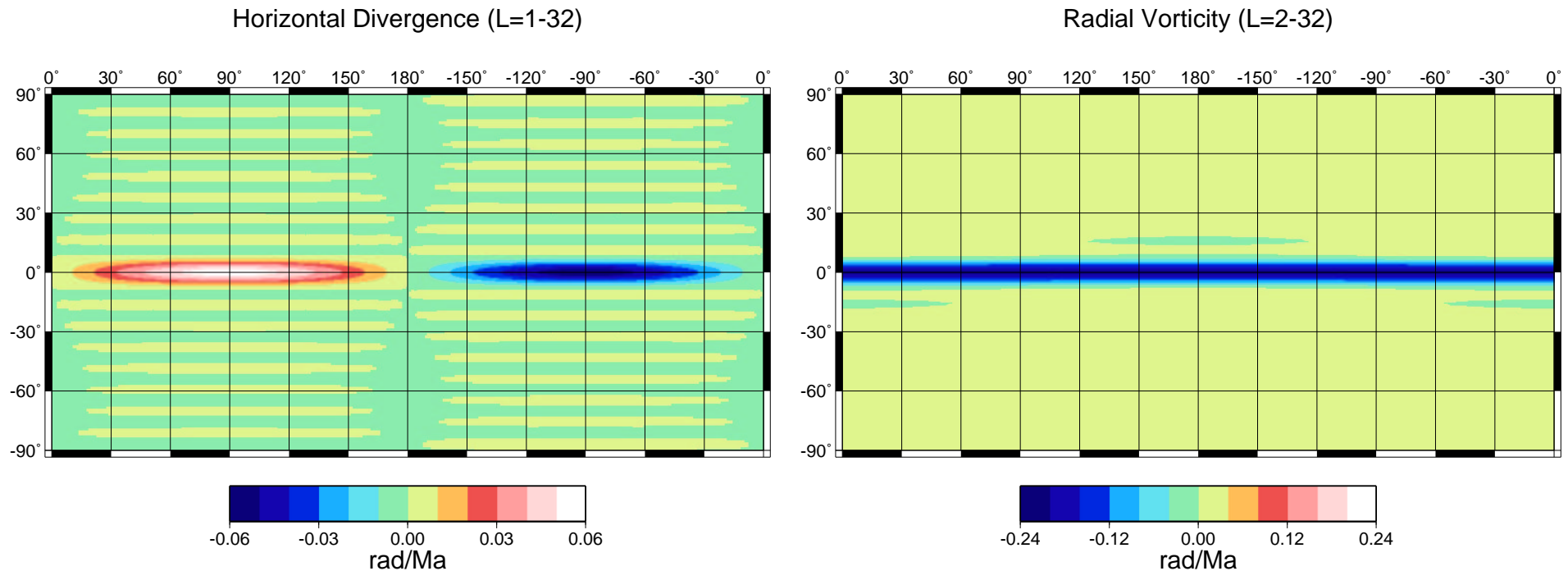
Fig. 3. Horizontal divergence and radial vorticity due to motion of hemispherical plates (eq. 27).

The *Gibbs oscillations* which are evident in Fig. 3 are due to the truncation of the spherical harmonic expansion of the discontinuous divergence and vorticity fields. We have suppressed the amplitude of these oscillations by multiplying the harmonic coefficients of the divergence and vorticity fields by the following

Lanczos smoothing factor (see *Lanczos*, 1961; *Justice*, 1978):

$$(\boldsymbol{\nabla}_H \cdot \mathbf{v})_\ell^m \rightarrow L_\ell^m \, (\boldsymbol{\nabla}_H \cdot \mathbf{v})_\ell^m \quad \text{and} \quad (\hat{\mathbf{r}} \cdot \boldsymbol{\nabla} \times \mathbf{v})_\ell^m \rightarrow L_\ell^m \, (\hat{\mathbf{r}} \cdot \boldsymbol{\nabla} \times \mathbf{v})_\ell^m$$

where

$$L_\ell^m = \left[\frac{\sin(m\pi/M)}{m\pi/M} \right] \left[\frac{\sin(\ell\pi/L)}{\ell\pi/L} \right] \tag{28}$$

The values of M and L may be set to the maximum harmonic degree and azimuthal order used in the truncated harmonic representation of the surface field. (In the case of Fig. 3, $L, M = 32$.)

2.3. Application to tectonic plates on Earth

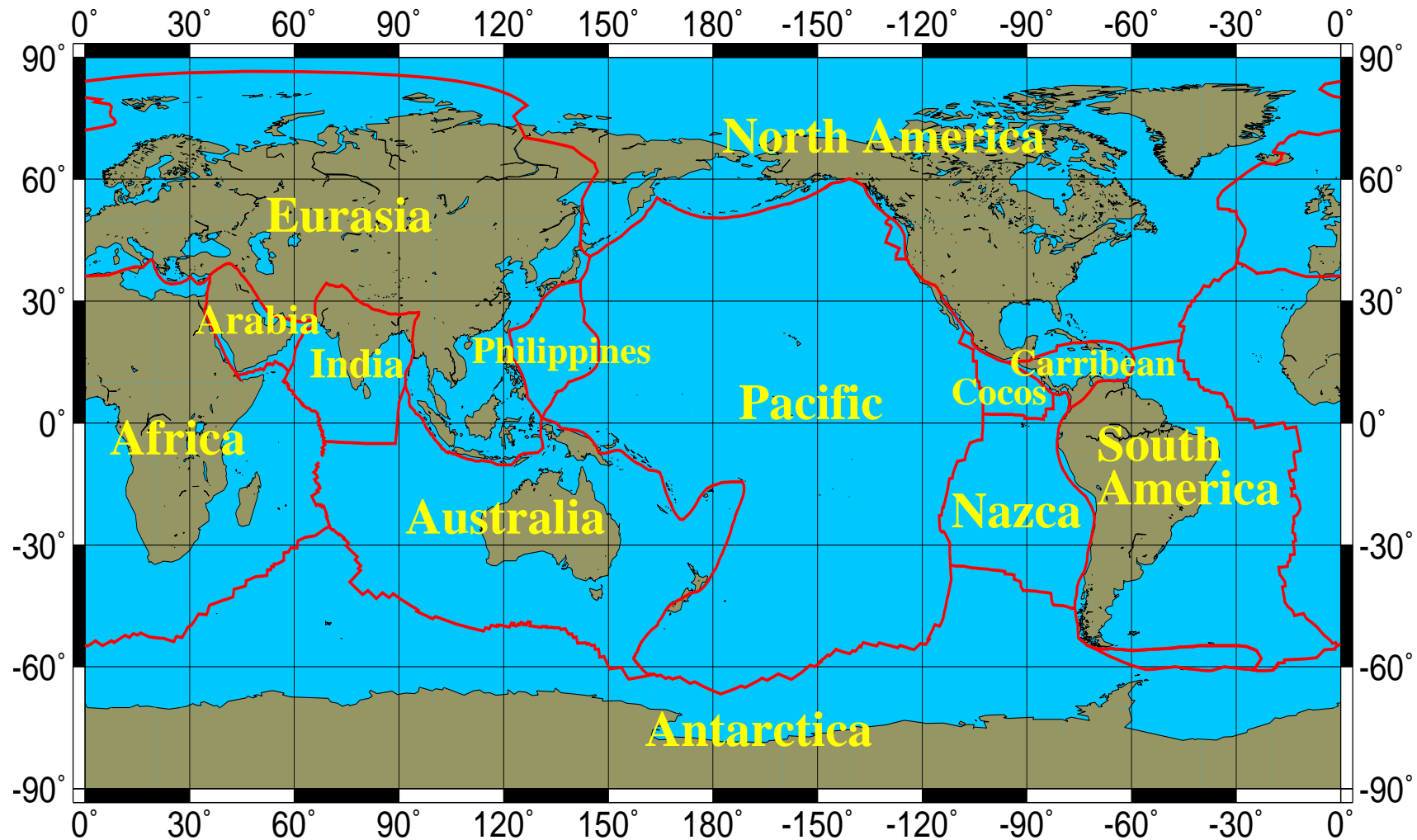We will now consider the application of expressions (22-23) to the observed tectonic plates on Earth's surface:

Fig. 4. The 13 main plates identified in *NUVEL-1* (*De Mets et al.*, 1990).

The amplitude spectrum of the function $H_i(\theta, \phi)$ describing the geometry of some of these tectonic plates is shown below in Fig. 5.
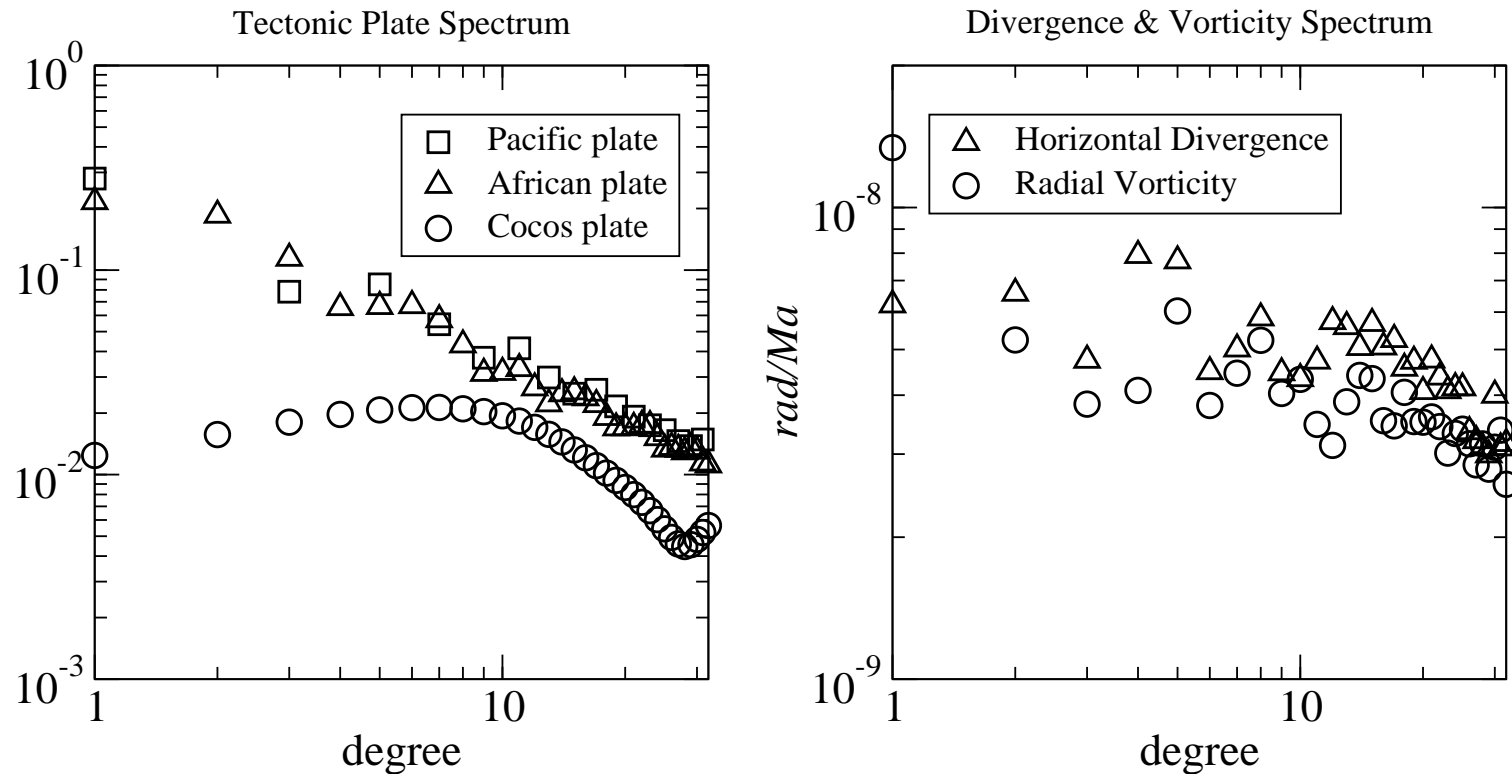
Fig. 5. Amplitude spectrum of the tectonic plates and the *NUVEL-1* divergence and vorticity spectrum.

The spectral amplitudes of the large Pacific and African plates display a $1/\ell$ variation which is similar to the hemispherical plates (Fig. 2). The small Cocos plate instead has a much flatter spectrum characteristic of a small disk (*i.e.,* similar to a 2-D delta function). The amplitude spectra of the corresponding plate divergence and vorticity fields, calculated using expressions (22-23) and using the relative rotation vectors in the *NUVEL-1* model (*De Mets et al.*, 1990), is

relatively flat, despite the fact that we used Lanczos smoothing (28) on these coefficients. The relatively flat divergence and vorticity spectra is similar to that obtained for the hemispherical plate motions (Fig. 2) because of the dominant contribution of the large plates (*e.g.,* Pacific and African). Fig. 5 shows that the strength of the plate vorticity field is nearly equal to that of the plate divergence. This *equipartition of energy* is also illustrated in the following maps:
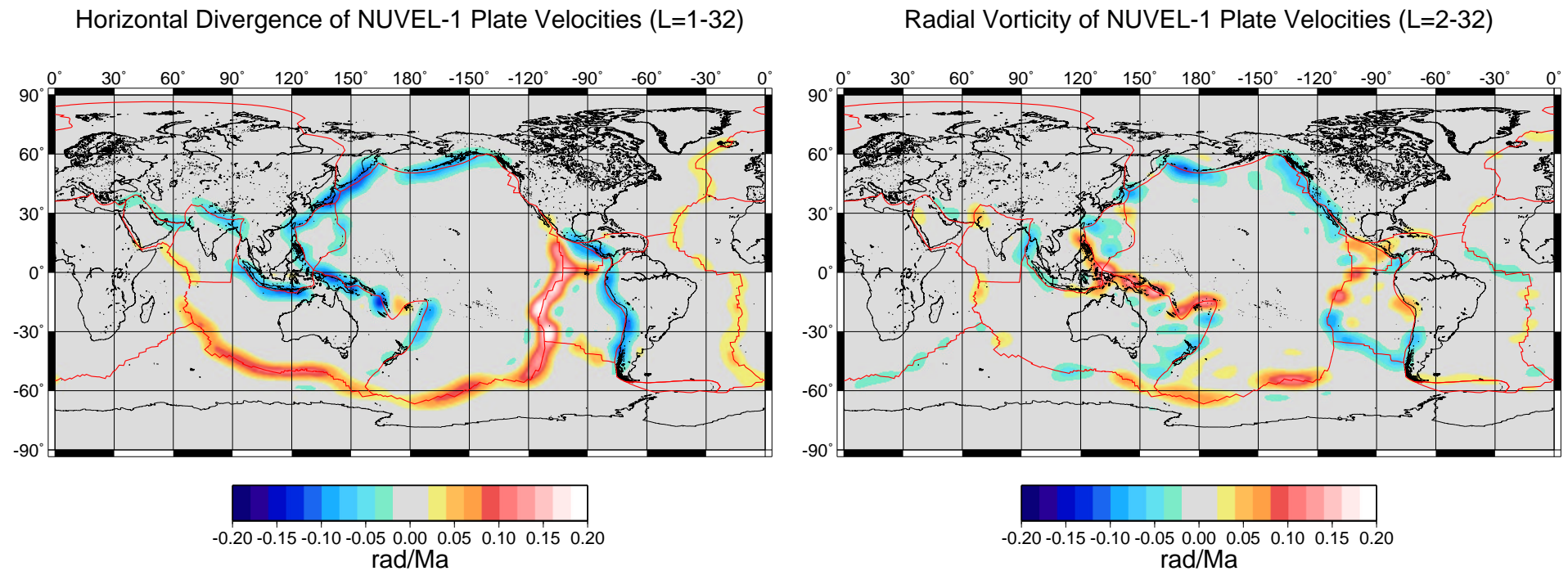

Fig. 6. Plate divergence and vorticity fields calculated using plate rotation vectors in *NUVEL-1* (*DeMets et al.,* 1990)

The Gibbs oscillations in the fields shown in Fig. 6 have again been suppressed

by using the Lanczos filtering in (28).

2.4. Poloidal-toroidal coupling generated by tectonic plates

The existence of rigid surface plates with weak boundaries is, in effect, an extreme manifestation of lateral variations of rheological properties in the lithosphere. As indicated in Lecture 1, the excitation of toroidal mantle flow requires the existence of lateral viscosity variations. This generation of toroidal flow arises through a viscous coupling with the buoyancy-induced poloidal flow in the mantle. The poloidal and toroidal mantle flows are manifested at the surface in terms of the horizontal divergence and radial vorticity of the plate motions. We will demonstrate how the presence of a finite number of rigid tectonic plates automatically requires the coupling of poloidal and toroidal surface flows.

We first note that expressions (22-23) may be rewritten as the following matrix equations:

$$d \;=\; \mathbf{S}\,\Delta\omega \tag{29}$$

$$\nu \;=\; \mathbf{R}\,\Delta\omega + \mathbf{T}\,\omega^N \tag{30}$$

in which $\boldsymbol{d}$ and $\boldsymbol{\nu}$ are column vectors containing the harmonic coefficients $(\boldsymbol{\nabla}_H \cdot \mathbf{v})^m_\ell$ and $(\hat{\mathbf{r}} \cdot \boldsymbol{\nabla} \times \mathbf{v})^m_\ell$, respectively, and the column vector $\boldsymbol{\Delta\omega}$ contains the $3(N-1)$ Cartesian components of the relative plate rotation vectors $\boldsymbol{\omega}^i - \boldsymbol{\omega}^N$. The matrices $\mathbf{S}$ and $\mathbf{R}$, which contain the elements $\left(S^i_j\right)^m_\ell$ and $\left(R^i_j\right)^m_\ell$, respectively (see eqs. 22-23), *depend only on the plate geometries.*

We may now represent the divergence matrix $\mathbf{S}$ in terms of its *singular value decomposition* (SVD) developed by *Lanczos* (1961):

$$\mathbf{S} = \mathbf{U}\underline{\boldsymbol{\Lambda}}\mathbf{V}^\mathsf{T} \tag{31}$$

in which $\mathbf{U}$ and $\mathbf{V}$ are orthonormal matrices (*i.e.,* $\mathbf{U}^\mathsf{T}\mathbf{U} = \mathbf{I} = \mathbf{V}^\mathsf{T}\mathbf{V}$) and $\underline{\boldsymbol{\Lambda}}$ is a *diagonal* matrix containing the *singular values* of the divergence matrix $\mathbf{S}$. [A useful, concise description of the Lanczos decomposition may be found in Volume II of *Aki & Richards* (1980).]

The dimensions of the matrices appearing in (31) are as follows:

$$\mathbf{S} \quad \rightarrow \quad L(L+2) \times 3(N-1)$$

$$\mathbf{U} \quad \rightarrow \quad L(L+2) \times 3(N-1)$$

$$\underline{\mathbf{\Lambda}} \quad \rightarrow \quad 3(N-1) \times 3(N-1)$$

$$\mathbf{V} \quad \rightarrow \quad 3(N-1) \times 3(N-1)$$

in which L is the maximum harmonic degree employed in the spherical harmonic representation of the plate divergence and vorticity fields. (In Figs. 5 and 6, $L = 32$.)

The columns of $\mathbf{V}$ constitute all the vectors which span the space of plate rotation vectors $\mathbf{\Delta\omega}$. If the singular values in $\underline{\mathbf{\Lambda}}$ are all nonzero, the columns of $\mathbf{V}$ span the entire space of rotation vectors and then $\mathbf{V}\,\mathbf{V}^\mathsf{T} = \mathbf{I}$.

The *generalized inverse* $\mathbf{S}^\mathrm{I}$ of the plate divergence matrix $\mathbf{S}$ is given by

$$\mathbf{S}^\mathrm{I} = \mathbf{V}\underline{\mathbf{\Lambda}}^{-1}\mathbf{U}^\mathsf{T} \tag{32}$$

Employing $\mathbf{S}^\mathrm{I}$, we can find the generalized inverse solution of eq. (29) and

thereby determine the particular plate rotation vectors $\boldsymbol{\Delta\omega}^{\mathrm{I}}$ which correspond to a given plate divergence field:

$$\boldsymbol{\Delta\omega}^{\mathrm{I}} = \mathbf{S}^{\mathrm{I}}\,\boldsymbol{d} \tag{33}$$

If one of more of the singular values in the diagonal matrix $\underline{\boldsymbol{\Lambda}}$ are zero, then there exists a family of plate rotations which will produce zero plate divergence. This *null family* of plate rotations is spanned by the columns of $\mathbf{V}$ which correspond to the zero singular values in $\underline{\boldsymbol{\Lambda}}$.In such a situation, the generalized inverse solution in (33) will only describe the restricted class of plate rotations which produce an nonzero plate divergence.

We can now establish the coupling which must exist between plate vorticity and divergence by substituting expression (33) into (30), and thereby obtain

$$\boldsymbol{\nu} = \mathbf{C}\,\boldsymbol{d}\; +\; \mathbf{T}\,\boldsymbol{\omega}^{N} \tag{34}$$

in which the coupling matrix, which depends only on plate geometry, is

$$\mathbf{C} = \mathbf{R}\,\mathbf{S}^{\mathrm{I}} \tag{35}$$

We therefore see that on a planet with rigid tectonic plates the horizontal divergence and radial vorticity are *not independent* and there is in fact a linear dependence between these two fields. The divergence-vorticity coupling expressed in (34) is controlled by the geometry of the tectonic plates. To the extent that the existence of the tectonic plates, and hence their geometry, is a manifestation of lateral variations of the rheology in the lithosphere, then equation (34) is an expression of the *poloidal-toroidal* coupling of flow in the lithosphere due to lateral viscosity variations.

3. Dynamical Models of Rigid Plate Motions Coupled to Mantle Flow

The mathematical and numerical difficulties involved in an explicit treatment of lateral viscosity variations, particularly the extreme variations associated with the surface tectonic plates, have motivated a number of studies which attempt to directly incorporate the observed plate motions into mantle flow models.

Hager & O'Connell (1981) developed the first such models in 3-D spherical geometry, in which the observed plate motions where directly imposed *via* the surface boundary conditions and they then attempted to balance the surface stresses generated by the imposed plate motions with the stresses generated by buoyancy forces inside the mantle. The primary internal driving forces considered were those due to the negative buoyancy of subducted slabs and, to a lesser extent, the small negative buoyancy associated with the cooling and thickening of the oceanic lithosphere.

The approach introduced by *Hager & O'Connell* (1981) was subsequently extended and modified by *Ricard & Vigny* (1989) for global flow in 3-D spherical geometry and by *Gable et al.* (1991) for numerical convection simulations in 3-D Cartesian geometry. The main modification was to avoid imposing *a priori* a

given set of plate motions, but rather to calculate the plate motions *a posteriori* in terms of the buoyancy forces inside the mantle. The basic approach, which is also used by *Hager & O'Connell* (1981), is to match the stresses exerted by buoyancy driven flow, acting on a no-slip surface, with the stresses arising from a prescribed plate velocity field with *unknown* plate rotation vectors. The rotation vectors are then determined *via* the stress matching.

In the models developed by *Ricard & Vigny* (1989) and by *Gable et al.* (1991), *it is assumed that all stresses acting on plate boundaries are zero*. This is a very questionable assumption since, as pointed out by *Hager & O'Connell* (1981), there are significant collision-related stresses at subduction zones and significant shear stresses along transform plate boundaries. Such difficulties led to the development of an alternative model of plate-coupled, buoyancy induced mantle flow which was first described in *Forte & Peltier* (1991). This alternative approach does not make any assumptions about the state of stress at plate boundaries and the plate motions are again determined on the basis of the internal buoyancy forces, rather than being imposed *a priori*. A detailed discussion of this approach will be provided below.

3.1. Theory of buoyancy driven plate motions

We begin by reconsidering the SVD (31) of the plate divergence matrix, which determines the relationship (29) between the surface plate divergence and the plate rotation vectors:

$$\boldsymbol{d} = \mathbf{U} \, \underline{\boldsymbol{\Lambda}} \, \mathbf{V}^{\mathsf{T}} \boldsymbol{\Delta\omega}$$

We immediately see from this expression that the harmonic coefficients of any realizable plate divergence field must be a linear superposition of the columns in matrix $\mathbf{U}$. We can therefore define the following *plate projection operator* $\mathbf{P}$:

$$\mathbf{P} = \mathbf{U} \, \mathbf{U}^{\mathsf{T}} \tag{36}$$

which acts on any *arbitrary* column vector $\boldsymbol{d}_0$ as follows

$$\mathbf{P}\boldsymbol{d}_0 = \boldsymbol{d}_1 \tag{37}$$

where $\boldsymbol{d}_1$ now contains the harmonic coefficients of a realizable field of plate divergence. Since the plate divergence matrix S is dependent only on the plate geometry, it immediately follows that the *projection operator* $\mathbf{P}$ *will also depend solely on the geometry of the surface plates.*

Recall from Lecture 1 (eq. 53), that the surface divergence of the buoyancy-induced mantle flow, predicted with a simple free-slip surface boundary condition, is given by the following expression:

$$(\boldsymbol{\nabla}_{\mathrm{H}} \cdot \mathbf{u})_{\ell}^{m} = \frac{g_o}{\eta_o} \int_{b}^{a} S_{\ell}(\eta(r)/\eta_o; r') \, \delta\rho_{\ell}^{m}(r') \, dr' \qquad (38)$$

in which the surface divergence kernel S_{ℓ} depends on the nondimensional radial viscosity profile $\eta(r)/\eta_o$ as well as on the radius. Since we have assumed free-slip conditions at the surface, *all* the internal density anomalies $\delta\rho$ in the mantle will contribute to the predicted surface flow, as is evident in expression (38). In general the predicted surface divergence will not look very 'plate-like', as we saw in Fig. 19 in Lecture 1.

We may obtain a 'plate-like' or realizable plate divergence field, $\boldsymbol{\nabla}_{\mathrm{H}} \cdot \mathbf{v}$, from the predicted field, $\boldsymbol{\nabla}_{\mathrm{H}} \cdot \mathbf{u}$, by applying the plate projection operator $\mathbf{P}$ introduced in (36-37):

$$(\boldsymbol{\nabla}_{\mathrm{H}} \cdot \mathbf{v})_{\ell}^{m} = \mathrm{P}_{\ell m, \, st} \, (\boldsymbol{\nabla}_{\mathrm{H}} \cdot \mathbf{u})_{s}^{t} \qquad (39)$$

in which the ordered pair $(\ell m, \, st)$ identify a particular row and column, respectively, of the plate projection matrix $\mathbf{P}$. It should be understood in (39) that

a sum over all values of $s\,t$ is implied on the right hand side of this equation. If we now combine expressions (38) and (39) we find

$$(\boldsymbol{\nabla}_{\mathrm{H}} \cdot \mathbf{v})_{\ell}^{m} = \frac{\mathrm{g}_{o}}{\eta_{o}} \int_{b}^{a} S_{\ell}(r')\, \delta\hat{\rho}_{\ell}^{m}(r')\, dr' \tag{40}$$

in which

$$\delta\hat{\rho}_{\ell}^{m}(r) = \left[S_{\ell}^{-1}(r)\, \mathrm{P}_{\ell m,\, st}\, S_{s}(r) \right] \delta\rho_{s}^{t}(r) \tag{41}$$

The density perturbations $\delta\hat{\rho}_{\ell}^{m}(r)$ defined in (41) give rise to a surface divergence field in (40) which is perfectly plate-like (*i.e.*, corresponds to a divergence produced by rigid-body rotations of the plates). By virtue of expression (41), we define the following *density projection operator* $\hat{\mathbf{P}}$:

$$\hat{\mathrm{P}}_{\ell m,\, st}(r) = S_{\ell}^{-1}(r)\, \mathrm{P}_{\ell m,\, st}\, S_{s}(r) \tag{42}$$

This density projection operator allows us to partition any arbitrary field of

mantle density anomalies $\delta\rho_s^t(r)$ into two *orthogonal families* as follows:

$$\delta\hat{\rho}_\ell^m(r) = \hat{P}_{\ell m,\, st}(r)\delta\rho_s^t(r) \tag{43}$$

$$\delta\bar{\rho}_\ell^m(r) = \left[\delta_{\ell m,\, st} - \hat{P}_{\ell m,\, st}(r)\right]\delta\rho_s^t(r) \tag{44}$$

in which $\delta_{\ell m,\, st}$ is simply an element of the identity matrix **I**. We can immediately establish that the density perturbations $\delta\hat{\rho}_\ell^m(r)$ in (43) and $\delta\bar{\rho}_\ell^m(r)$ in (44) belong to orthogonal families by noting that:

$$\hat{P}_{\ell m,\, st}(r)\, \delta\hat{\rho}_s^t(r) = \delta\hat{\rho}_\ell^m(r) \tag{45}$$

$$\hat{P}_{\ell m,\, st}(r)\, \delta\bar{\rho}_s^t(r) = 0 \tag{46}$$

The family of density perturbations $\delta\hat{\rho}$ in (43) can produce realizable surface plate motions whereas the family $\delta\bar{\rho}$ cannot produce a plate-like surface flow field. The mantle flow driven by the density anomalies $\delta\hat{\rho}$ should thus be modelled with a *free-slip* surface boundary condition, while the flow driven by $\delta\bar{\rho}$ should be modelled with a *no-slip* surface. The tectonic plates are effectively 'locked' into position by the flow driven by $\delta\bar{\rho}$, acting as a rigid 'lid'.

The family of density perturbations $\delta\bar{\rho}$ constitutes the portion of internal buoyancy forces which are completely 'invisible' from the perspective of the tectonic plate motions. This conclusion has important consequences for any effort to reconstruct the density perturbations in the mantle, solely on the basis on past and present-day plate motions (*e.g., Richards & Engebretson,* 1992; *Ricard et al.,* 1993). Any such effort, for example to reconstruct the subducted slab heterogeneity from past plate motions, will suffer from a fundamental nonuniqueness owing to the existence of the $\delta\bar{\rho}$ family of density anomalies.

3.2. Predicting plate motions with tomography-based flow models

We will now illustrate an application of the theory of buoyancy-induced plate motions to tomography-based mantle flow models. Unless stated otherwise, all calculations will be based on the recent high-resolution model of global S-wave heterogeneity derived by *Grand* (2002). The principal inputs needed to carry out the mantle flow calculation are the mantle viscosity profile and the velocity-to-density scaling profile $d \ln \rho / d \ln V_s$. The mantle viscosity profile we will employ (Fig. 7) has recently been derived by *Mitrovica & Forte* (2004) on the basis of a nonlinear, Occam inversion (*Constable et al.,* 1987) of a combined set of

postglacial rebound and convection data. The convection data included the present-day plate divergence field which was modelled in terms of the plate-like mantle flow theory described above. The $d \ln \rho / d \ln V_s$ scaling profile (Fig. 7) was similarly derived by carrying out an Occam inversion of the convection-related surface data (*i.e.,* global free-air gravity anomalies, dynamic surface topography, observed plate divergence and the excess or dynamic CMB ellipticity).

The density projection operator (eq. 42) was calculated on the basis of the geometry of the 13 major tectonic plates (Fig. 4) and using the surface divergence kernels calculated on the basis of the Occam-inferred viscosity profile. These kernels are illustrated in Fig. 7 below.
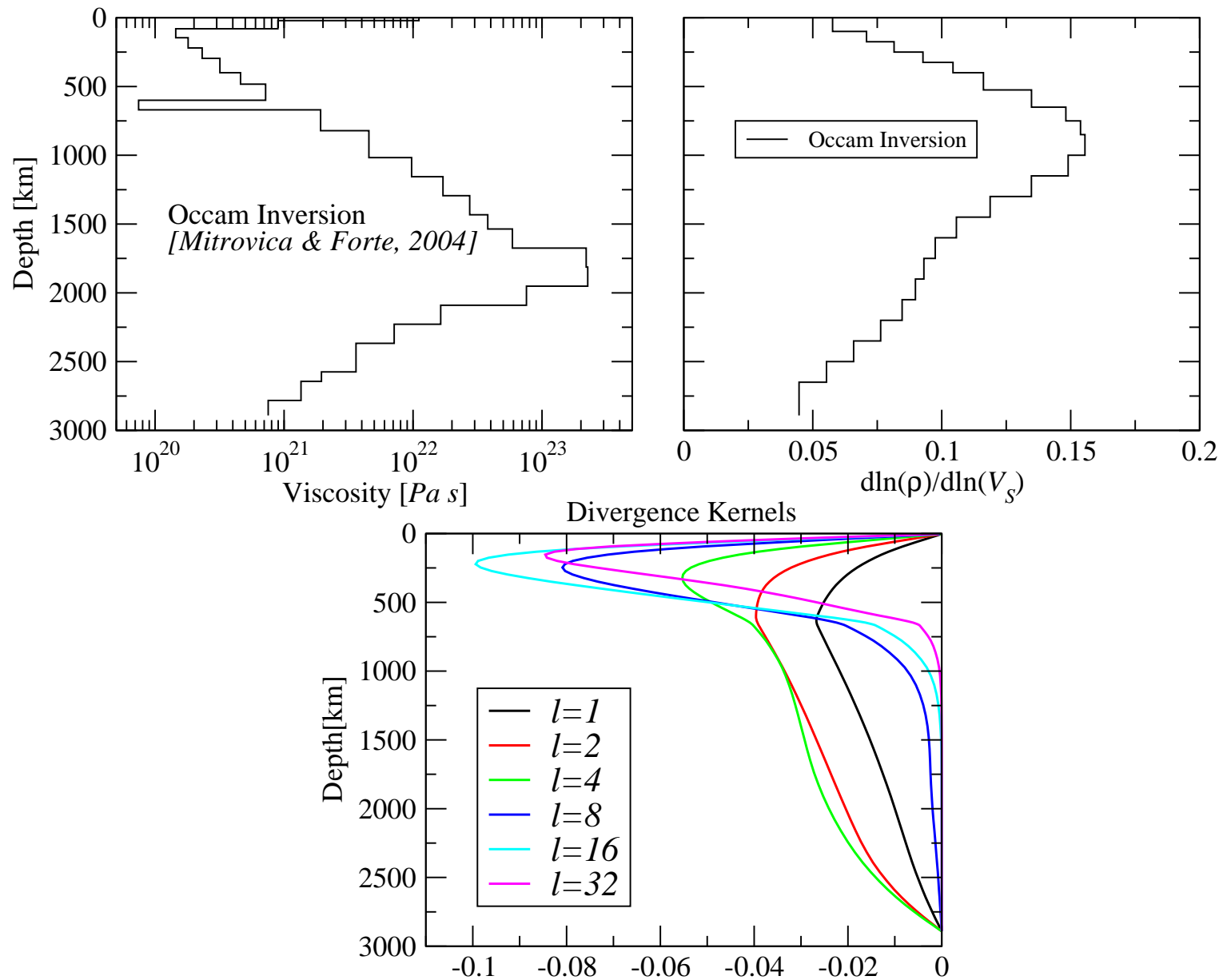
Fig. 7. The principal geodynamic inputs required to model the buoyancy driven surface flow.

We now have all the ingredients to explore the impact of the rigid surface plates on the buoyancy-driven mantle flow. The surface divergence predicted in the absence of tectonic plates, assuming a simple free-slip surface boundary condition, is shown below (Fig. 8). We again note that the predicted surface divergence is far from appearing plate-like.

It is interesting to next consider the impact of two hemispherical plates (Fig. 1) on the predicted surface divergence (Fig. 8). We can immediately observe that overall amplitude of the predicted surface divergence is nearly two orders of magnitude smaller than the free-slip prediction. This example shows the importance of the geographical alignment between the plate-boundary geometry and the geometry of the upwellings and downwellings in the mantle. It is clear in this example that the plates are essentially 'locked' in response to the underlying buoyancy driven flow.

The final calculation was carried with the present-day tectonic plate geometry (Fig. 4) and we now note that the overall amplitude of the predicted plate-like divergence is only a factor of two smaller than the free-slip prediction. Evidently, the plates are favourably aligned with respect to the predicted underlying mantle flow.
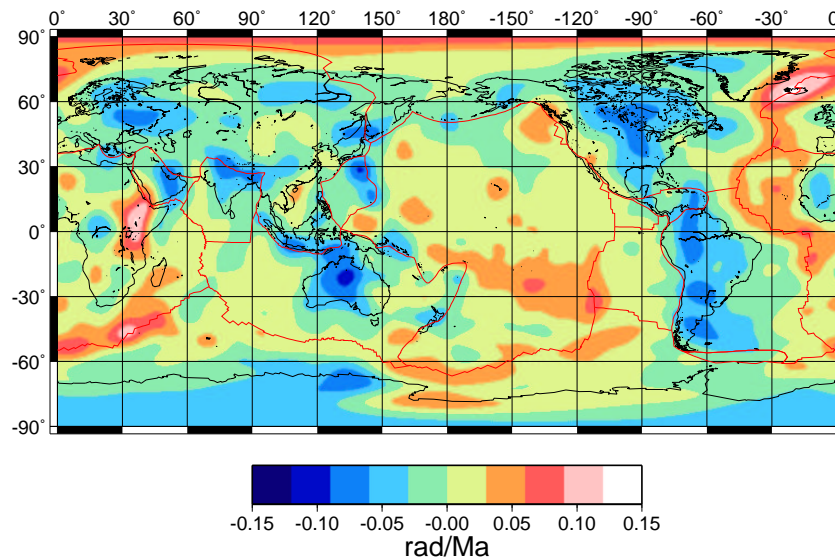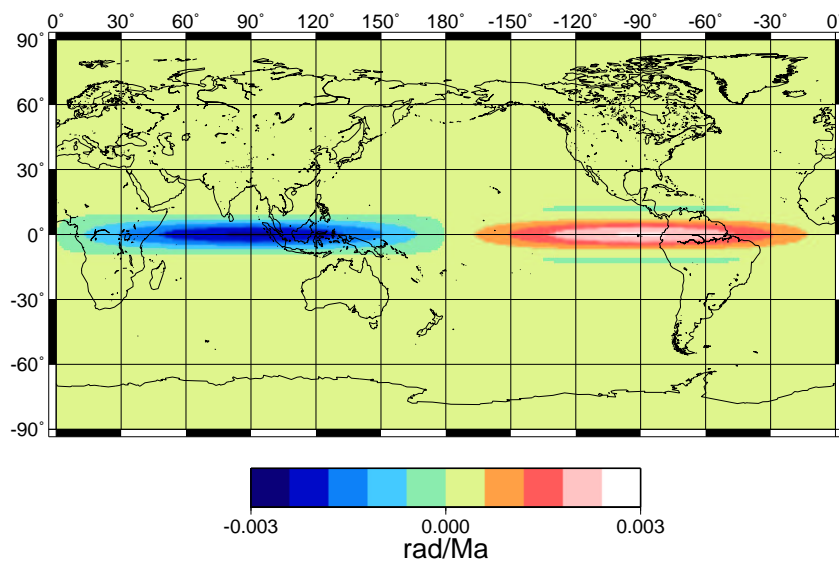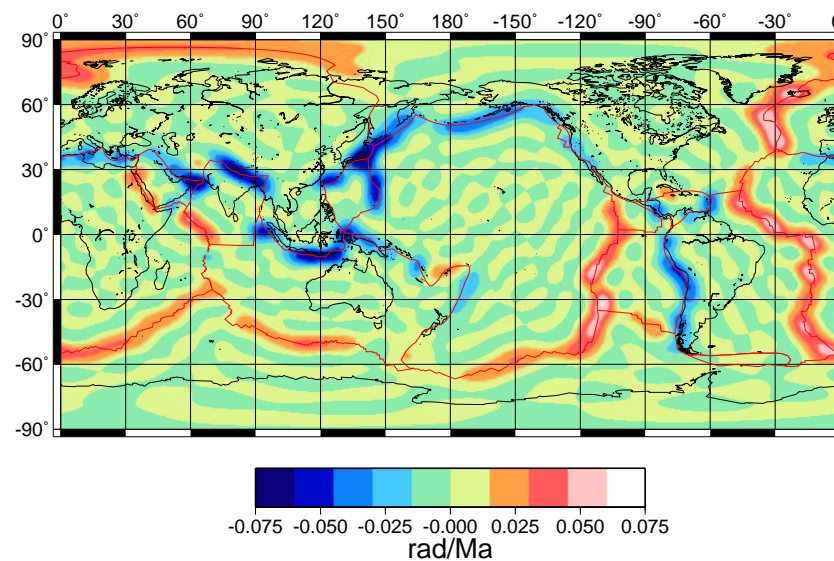
Fig. 8. Surface divergence predicted in absence of plates, with 2 hemispherical plates and with the 13 major, present-day tectonic plates. Internal mantle flow predicted using *Grand*'s (2002) tomography model.

4. Variational Modelling of Mantle Flow with Lateral Viscosity Variations

The treatment of rigid surface plates and their impact on the buoyancy induced mantle flow, described in the previous section, is very convenient because it allows us to treat the plate-like structure of the lithosphere without explicitly modelling the lateral variations in rheology associated with the plates. This technique only introduces the effect of plates as a surface boundary condition, via the use of the plate-projection operator (42). The dynamical details of the coupling between poloidal and toroidal flows is however not determined explicitly. A complete, dynamically consistent treatment of the effect of lateral viscosity variations and the resulting poloidal-toroidal flow coupling must be based on the solution of the momentum conservation equation (8) derived in the Introduction.

The direct mathematical solution of differential equation (8) is rather complicated. One possibility is of course to write an equivalent finite-difference approximation to the equation and solve the resulting equations numerically. Finite-element solutions in 2-D Cartesian geometry were presented by

Christensen (1984) and later extended to 3-D Cartesian geometry by *Christensen & Harder* (1991). The extension of finite-element numerical solutions to 3-D spherical geometry is well illustrated by the study of *Zhong et al.* (1998).

Interesting alternatives to the purely numerical solutions of mantle flow with lateral viscosity variations have been presented by *Ribe* (1992) and by *Zhang & Christensen* (1993). In the former study, a thin-shell approximation is used, in which lateral viscosity variations are only considered in the lithosphere. In the latter study, the spectral propagator solutions for mantle flow in 3-D spherical geometry (described in Lecture 1) were modified to allow for the presence of lateral viscosity variations throughout the mantle.

Variational methods provide a mathematically elegant solution which can also provide useful physical insight into the dynamics of poloidal-toroidal flow coupling. The initial application of variational problems to mantle-flow in spherical geometry was presented by *Čadek et al.* (1993) and is based on the use of an iterative numerical scheme. A direct and quasi-analytic solution was presented by *Forte* (1992) and is described in detail in *Forte & Peltier* (1994). In this section we will consider the approach presented in the latter reference.

4.1. A variational principle for buoyancy induced mantle flow

We begin with the equations (3-4) expressing momentum conservation and the constitutive relation for an extremely viscous (*i.e.*, infinite Prandtl number) fluid:

$$\partial_k \sigma_{ki} + \rho_o \partial_i \phi_1 + \rho_1 \partial_i \phi_o = 0 \tag{47}$$

in which

$$\sigma_{ij} = -P_1 \delta_{ij} + 2\eta E_{ij} \text{ , where } E_{ij} = \frac{1}{2}(\partial_i u_j + \partial_j u_i - \frac{2}{3}\delta_{ij}\partial_k u_k) \tag{48}$$

If we further assume for simplicity that the fluid is incompressible, we then have the following expression for mass conservation (see Lecture 1):

$$\partial_k u_k = 0 \tag{49}$$

Equations (47-49) describe a flow field u_i driven by density perturbations ρ_1 which are assumed to be known *a priori* and are henceforth treated as fixed. This buoyancy induced flow field occurs in a bounded spatial volume V with a surface boundary S. The boundary conditions which the flow field u_i must

satisfy are:

$$\hat{n}_i u_i = 0 \tag{50}$$

$$\hat{h}_i \hat{n}_j \sigma_{ji} = 0 \ \text{ on } S_1 \tag{51}$$

$$u_i = c_i \ \text{ on } S_2 \tag{52}$$

where $\hat{n}_i$ is the unit vector everywhere normal to the surface S, $\hat{h}_i$ is any unit vector which is tangential to the surface S, S_1 is the portion of the bounding surface on which *free-slip* (*i.e.*, zero tangential stress) conditions apply and S_2 (= $S - S_1$) is the portion on which the *horizontal velocity* c_i is prescribed.

Let us assume that we posses a *particular solution* u_i to the governing equations (47-49) and that this solution satisfies the boundary conditions (50-52). We now consider a *kinematically admissible* flow perturbation δu_i which satisfies mass conservation (49). The flow perturbation must be such that the total flow field $u_i + \delta u_i$ also satisfies the same boundary conditions (50-52) which are satisfied by the solution u_i. By taking the inner product of the flow perturbation δu_i with

the momentum conservation equation (47) we obtain:

$$\partial_k(\sigma_{ki}\,\delta u_i) - \sigma_{ki}\,\partial_k(\delta u_i) + \partial_i(\rho_o\phi_1\,\delta u_i) + \rho_1(\partial_i\phi_o)\,\delta u_i = 0$$

in which we have used the result $\partial_k(\delta u_k) = 0$. If we now integrate this last expression over the entire volume V occupied by the fluid we obtain, by virtue of Gauss' theorem,

$$\int_V [\rho_1\partial_i\phi_o\,\delta u_i - \sigma_{ki}\,\delta E_{ki}]\,\mathrm{d}V + \int_S [\hat{n}_k\sigma_{ki}\,\delta u_i + \rho_o\phi_1\,\hat{n}_k\delta u_k]\,\mathrm{d}S = 0 \quad (53)$$

in which we have also used the result $\sigma_{ki}\partial_k\,\delta u_i = \sigma_{ki}\,\delta E_{ki}$ which follows from the symmetry of the stress tensor σ_{ki}.

Since both the solution u_i and the perturbed flow $u_i + \delta u_i$ satisfy the same boundary conditions on the surface S, it follows from (50) that

$$\hat{n}_k\,\delta u_k = 0\,, \text{ everywhere on } S \quad (54)$$

which implies that δu_i must be tangential to surface S. By virtue of the condition

(51) we therefore have that

$$\hat{n}_k \sigma_{ki}\, \delta u_i = 0 \;,\;\; \text{on } S_1 \tag{55}$$

Condition (52) also implies that

$$\delta u_i = 0 \;,\;\; \text{on } S_2 \tag{56}$$

From these three boundary conditions on the flow perturbation δu_i we can conclude that the surface integral in expression (53) must vanish and we therefore obtain

$$\int_V [\rho_1 \partial_i \phi_o\, \delta u_i - 2\eta E_{ki}\, \delta E_{ki}]\, \mathrm{d}V = 0 \tag{57}$$

in which we have used the result $P_1 \delta_{ki}\, \delta E_{ki} = P_1 \delta E_{kk} = 0$ by virtue of the incompressibility (49). Since the density anomalies ρ_1 and the reference gravity field ϕ_o are known *a priori,* we can then rewrite expression (57) as

$$\delta W = 0 \;,\;\; \text{where } W = \int_V [\eta E_{ij} E_{ij} - \rho_1 \partial_i \phi_o u_i]\, \mathrm{d}V \tag{58}$$

In other words, the functional W is *stationary* with respect to perturbations of the flow field *if and only if* the flow field u_i satisfies the governing equations (47-49) and all the boundary conditions (50-52). The functional W is the difference between the *rate of viscous dissipation of energy*, $\eta E_{ij} E_{ij}$, and the rate of *energy release by buoyancy*, $\rho_i \partial_i \phi_o u_i$.

It is important to note that in deriving the variational equation (58), we have assumed that the viscosity η is not a function of the flow field u_i (*i.e.*, $\delta\eta = 0$). This is equivalent to assuming a *linear, stress-independent, Newtonian rheology*. An extension of the variational principle for the case of stress-dependent rheology, which requires an iterative approach, may be found in the study by *Čadek et al.* (1993).

We can show that the functional W in expression (58) *must be an absolute minimum* for the flow field. To show this, let u_i^0 be the flow solution which satisfies $\delta W = 0$ and let u_i^1 be any kinematically admissible flow which satisfies mass conservation (49) and the boundary conditions (54-56). We may therefore express the perturbed flow field as $u_i = u_i^0 + \epsilon u_i^1$, in which $\epsilon \ll 1$, and therefore

the quantity W in (58) may be written as:

$$W = \int_V \left[\eta E_{ij}^0 E_{ij}^0 - \rho_1 \partial_i \phi_o u_i^0 \right] \, \mathrm{d}V$$

$$+ \epsilon \int_V \left[2\eta E_{ij}^0 E_{ij}^1 - \rho_1 \partial_i \phi_o u_i^1 \right] \, \mathrm{d}V$$

$$+ \epsilon^2 \int_V \left[\eta E_{ij}^1 E_{ij}^1 \right] \, \mathrm{d}V$$

From this expression we may regard W as a function of the perturbation variable ϵ:

$$W(\epsilon) = W(0) + \left(\frac{dW}{d\epsilon} \right)_0 \epsilon + \frac{1}{2} \left(\frac{d^2 W}{d\epsilon^2} \right)_0 \epsilon^2 \tag{59}$$

According to the variational principle (58), $\delta W = 0$, and therefore from expression (59) we have

$$\delta W = \left(\frac{dW}{d\epsilon} \right)_0 \delta \epsilon = 0 \, , \text{ which implies } \left(\frac{dW}{d\epsilon} \right)_0 = 0$$

We may therefore conclude that the functional $W(\epsilon)$ may be written as

$$W(\epsilon) = W(0) + \frac{1}{2}\left(\frac{d^2 W}{d\epsilon^2}\right)_0 \epsilon^2 \;,\quad \text{where} \quad \left(\frac{d^2 W}{d\epsilon^2}\right)_0 = 2\int_V \eta E_{ij}^1 E_{ij}^1 \, dV \quad (60)$$

The last term in expression (60) is *positive definite* and therefore it is clear that $W(0)$ must be the absolute minimum of the function $W(\epsilon)$. This minimum principle is simply an extension of the classical *minimum dissipation theorem* of Helmholtz [see pp. 227-228 in *Batchelor* (1967)] to fluids with internal buoyancy sources.

4.2. Variational calculation of buoyancy induced flow in 3-D spherical geometry

The calculation of buoyancy induced flow in spherical geometry, using the variational principle (58), can be greatly facilitated by using the *generalized spherical harmonics* described in *Phinney & Burridge* (1973), henceforth referred to as PB for convenience.

We begin by expressing the tensor inner product $E_{ij}E_{ij}$ in terms of the so-called

contravariant canonical components presented in PB:

$$E_{ij}E_{ij} = C_{i\alpha}C_{j\beta}E^{\alpha\beta}C_{i\gamma}C_{j\delta}E^{\gamma\delta} = e_{\alpha\gamma}e_{\beta\delta}E^{\alpha\beta}E^{\gamma\delta}$$

$$= E^{00}E^{00} + 2E^{++}E^{--} + 2E^{+-}E^{+-} - 4E^{0+}E^{0-} \qquad (61)$$

The Latin indices $i = 1, 2, 3$ refer to the coordinate directions $(\hat{\boldsymbol{\vartheta}}, \hat{\boldsymbol{\varphi}}, \hat{\boldsymbol{r}})$, respectively. The Greek indices $\alpha = -1, 0, +1$ refer the complex coordinate directions $(\hat{\boldsymbol{e}}_-, \hat{\boldsymbol{e}}_0, \hat{\boldsymbol{e}}_+)$, respectively (see Lecture 1). The unitary rotation matrix $C_{i\alpha}$ which relates these two coordinate systems is:

$$C_{i\alpha} = \begin{pmatrix} \frac{1}{\sqrt{2}} & 0 & -\frac{1}{\sqrt{2}} \\ -\frac{\imath}{\sqrt{2}} & 0 & -\frac{\imath}{\sqrt{2}} \\ 0 & 1 & 0 \end{pmatrix} \qquad (62)$$

in which $\imath = \sqrt{-1}$.

The contravariant strain-rate tensor components in (61) are defined as

$$E^{\alpha\beta} = \frac{1}{2}\left[u^{\alpha,\beta} + u^{\beta,\alpha}\right]$$

$$= \frac{1}{2}\sum_{\ell=0}^{\infty}\sum_{m=-\ell}^{+\ell}\left[U_{\ell}^{(\alpha|\beta)\,m}(r) + U_{\ell}^{(\beta|\alpha)\,m}(r)\right]Y_{\ell}^{(\alpha+\beta)\,m}(\theta,\phi) \qquad (63)$$

Employing the covariant differentiation rules in PB to evaluate the terms $U_{\ell}^{(\alpha|\beta)\,m}(r)$ in expression (63), we obtain the following:

$$E^{00} = \sum_{\ell\,m}(E_1)_{\ell}^{m}\,Y_{\ell}^{0\,m}, \quad E^{+-} = \sum_{\ell\,m}(E_2)_{\ell}^{m}\,Y_{\ell}^{0\,m}, \qquad E^{0+} = \sum_{\ell\,m}(E_3)_{\ell}^{m}\,Y_{\ell}^{1\,m}$$

$$E^{0-} = \sum_{\ell\,m}(E_4)_{\ell}^{m}\,Y_{\ell}^{-1\,m}, \quad E^{++} = \sum_{\ell\,m}(E_5)_{\ell}^{m}\,Y_{\ell}^{2\,m}, \quad E^{--} = \sum_{\ell\,m}(E_6)_{\ell}^{m}\,Y_{\ell}^{-2\,m}$$

$$(64)$$

in which

$$(E_1)_\ell^m = \frac{d}{dr} U_\ell^{0\,m} \;,\; (E_2)_\ell^m = \frac{\Omega_1^\ell}{2r} \left[U_\ell^{+\,m} + U_\ell^{-\,m} \right] - \frac{1}{r} U_\ell^{0\,m}$$

$$(E_3)_\ell^m = \frac{1}{2} \left(\frac{d}{dr} - \frac{1}{r} \right) U_\ell^{+\,m} + \frac{\Omega_1^\ell}{2r} U_\ell^{0\,m} \;,\; (E_4)_\ell^m = \frac{1}{2} \left(\frac{d}{dr} - \frac{1}{r} \right) U_\ell^{-\,m} + \frac{\Omega_1^\ell}{2r} U_\ell^{0\,m}$$

$$(E_5)_\ell^m = \frac{\Omega_2^\ell}{r} U_\ell^{+\,m} \;,\; (E_6)_\ell^m = \frac{\Omega_2^\ell}{r} U_\ell^{-\,m} \tag{65}$$

in which $U_\ell^{\alpha\,m}(r)$ is the generalized spherical harmonic coefficient of the contravariant flow component u^α:

$$u^\alpha(r,\theta,\phi) = \sum_{\ell,m} U_\ell^{\alpha\,m}(r)\, Y_\ell^{\alpha\,m}(\theta,\phi)$$

and

$$\Omega_1^\ell = \sqrt{\frac{\ell(\ell+1)}{2}} \;,\; \Omega_2^\ell = \sqrt{\frac{(\ell-1)(\ell+2)}{2}}$$

We now require expressions for the contravariant flow coefficients $U_\ell^{\alpha\,m}(r)$ in terms of the *poloidal* and *toroidal* flow scalars. Recall (Lecture 1) that *Backus* (1958)

proved any incompressible flow field **u** may be written as:

$$\mathbf{u} = \boldsymbol{\nabla} \times \boldsymbol{\Lambda} p + \boldsymbol{\Lambda} q \ , \ \text{where} \ \boldsymbol{\Lambda} = \mathbf{r} \times \boldsymbol{\nabla} \tag{66}$$

in which p and q are the poloidal and toroidal flow scalars, respectively. The contravariant flow components u^α may be obtained from the components u_i in (66) by using the relation

$$u^\alpha = C^\dagger_{\alpha i} \, u_i \tag{67}$$

where $C^\dagger_{\alpha i}$ is the Hermitian conjugate of the unitary rotation matrix $C_{i\alpha}$ in (62). By substituting expression (66) into (67) we find:

$$U_\ell^{0\ m}(r) = -\frac{2(\Omega_1^\ell)^2}{r} p_\ell^m(r)$$

$$U_\ell^{-\ m}(r) = -\Omega_1^\ell \left(\frac{1}{r} \frac{d}{dr} r p_\ell^m(r) + \imath q_\ell^m(r) \right) \tag{68}$$

$$U_\ell^{+\ m}(r) = -\Omega_1^\ell \left(\frac{1}{r} \frac{d}{dr} r p_\ell^m(r) - \imath q_\ell^m(r) \right)$$

in which $\imath = \sqrt{-1}$ and $p_\ell^m(r)$, $q_\ell^m(r)$ are the (ordinary) spherical harmonic

coefficients of the poloidal and toroidal flow scalars, respectively.

We allow for explicit 3-D variations in viscosity by expanding the viscosity $\eta(r, \theta, \phi)$ as follows:

$$\eta(r, \theta, \phi) = \sum_{\ell, m} \eta_\ell^m(r) Y_\ell^m(\theta, \phi) \tag{69}$$

We now have all the elements needed to calculate the dissipation integral

$$\int_V \eta E_{ij} E_{ij} \, \mathrm{d}V$$

which appears in the variational principle (58). By combining expressions (61, 64, 65, 68, 69) we can show that:

$$\int_V \eta E_{ij} E_{ij} \, dV = 4\pi \sum_{\ell,m} \sum_{s,t} \sum_{J=|\ell-s|}^{\ell+s} \sqrt{(2\ell+1)(2s+1)(2J+1)} \begin{pmatrix} \ell & s & J \\ m & t & -m-t \end{pmatrix}$$

$$\times \int_b^a \eta_J^{-m-t}(r) \left\{ \begin{pmatrix} \ell & s & J \\ 0 & 0 & 0 \end{pmatrix} \frac{6(\Omega_1^\ell)^2 (\Omega_2^s)^2}{r^2} \left[\frac{dp_\ell^m}{dr} - \frac{p_\ell^m}{r} \right] \left[\frac{dp_s^t}{dr} - \frac{p_s^t}{r} \right] + \right.$$

$$\begin{pmatrix} \ell & s & J \\ 2 & -2 & 0 \end{pmatrix} \frac{2\Omega_1^\ell \Omega_2^\ell \Omega_1^s \Omega_2^s}{r^2} \left[\frac{dp_\ell^m}{dr} + \frac{p_\ell^m}{r} - \imath q_\ell^m \right] \left[\frac{dp_s^t}{dr} + \frac{p_s^t}{r} + \imath q_s^t \right] -$$

$$\begin{pmatrix} \ell & s & J \\ 1 & -1 & 0 \end{pmatrix} \Omega_1^\ell \Omega_1^s \left[\frac{d^2 p_\ell^m}{dr^2} + \frac{2(\Omega_2^\ell)^2 \, p_\ell^m}{r^2} - \imath r \frac{d}{dr} \left(\frac{q_\ell^m}{r} \right) \right] \times$$

$$\left. \left[\frac{d^2 p_s^t}{dr^2} + \frac{2(\Omega_2^s)^2 \, p_s^t}{r^2} + \imath r \frac{d}{dr} \left(\frac{q_s^t}{r} \right) \right] \right\} \, r^2 \, dr \qquad (70)$$

We note the appearance of *Wigner 3-j* symbols in the dissipation integral (70). These 3-j symbols were used to express the coupling between two generalized

spherical harmonics as follows:

$$Y_{\ell_1}^{N_1 m_1}(\theta, \phi)\, Y_{\ell_2}^{N_2 m_2}(\theta, \phi) = \sum_{\ell=|\ell_1-\ell_2|}^{\ell_1+\ell_2} \sqrt{(2\ell_1+1)(2\ell_2+1)(2\ell+1)} \times$$

$$\begin{pmatrix} \ell_1 & \ell_2 & \ell \\ N_1 & N_2 & N \end{pmatrix} \begin{pmatrix} \ell_1 & \ell_2 & \ell \\ m_1 & m_2 & m \end{pmatrix} Y_{\ell}^{Nm}(\theta, \phi)^* \quad (71)$$

in which the the asterisk $*$ denotes complex conjugation. A summary of useful aspects of spherical harmonic coupling rules, in the context of fluid dynamics in spheres, can be found in *Forte & Peltier* (1994, Appendix II).

By expanding the mantle density anomalies $\rho_1(r, \theta, \phi)$ in terms of spherical harmonics, the buoyancy integral which appears in the variational principle (58) may be written as:

$$\int_V \rho_1 \partial_i \phi_o u_i \, \mathrm{d}V = -4\pi \sum_{\ell, m} \int_b^a (\rho_1)_\ell^m(r)^* \, U_\ell^{0\,m}(r) \, \mathrm{g}_o(r) \, r^2 \, dr$$

By virtue of expression (68), this last expression may be rewritten as:

$$\int_V \rho_1 \partial_i \phi_o u_i \, dV = 4\pi \sum_{\ell,m} 2(\Omega_1^\ell)^2 \int_b^a \frac{(\rho_1)_\ell^m (r)^*}{r} \, p_\ell^m (r) \, g_o(r) \, r^2 \, dr \qquad (72)$$

The variational principle (58) requires that we minimize the functional W with respect to the flow field. To accomplish this minimization, we expand the spherical harmonic components of the poloidal and toroidal flow scalars in terms of radial basis functions as follows:

$$\begin{aligned} p_\ell^m (r) &= \sum_{n=1}^N {}_n p_\ell^m \, f_n(r) \\ q_\ell^m (r) &= \sum_{n=1}^N {}_n q_\ell^m \, g_n(r) \end{aligned} \qquad (73)$$

The radial basis functions $f_n(r)$ and $g_n(r)$ must satisfy the boundary conditions (50-52). When the expansions (73) are inserted into the dissipation (70) and buoyancy (72) integrals, the functional W in expression (58) will vary according to the values of the scalar coefficients ${}_n p_\ell^m$ and ${}_n q_\ell^m$ in (73). *The particular values of these radial coefficients which minimizes the functional W defines the flow solution.* We may therefore conclude that the functional W will be a minimum when the

following conditions are satisfied:

$$\frac{\partial W}{\partial(_np_s^t)} = \frac{\partial}{\partial(_np_s^t)} \int_V \left[\eta E_{ij} E_{ij} - \rho_1 \partial_i \phi_o u_i \right] \, \mathrm{d}V = 0 \tag{74}$$

$$\frac{\partial W}{\partial(_nq_s^t)} = \frac{\partial}{\partial(_nq_s^t)} \int_V \left[\eta E_{ij} E_{ij} \right] \, \mathrm{d}V = 0 \tag{75}$$

The set of coefficients which satisfy equations these two conditions will describe the flow solution we seek.

The substitution of expansions (73) into the dissipation (70) and buoyancy (72) integrals, followed by the application of conditions (74-75) will yield the following coupled set of algebraic equations:

$$\sum_{k,\ell,m} A_{nst}^{k\ell m} \, _kp_\ell^m + \sum_{k,\ell,m} B_{nst}^{k\ell m} \, _kq_\ell^m = \frac{2(\Omega_1^s)^2}{\eta_o} \int_b^a \frac{(\rho_1)_s^t(r)^*}{r} \, f_n(r) \, \mathrm{g}_o(r) \, r^2 \, dr$$

$$\tag{76}$$

$$\sum_{k,\ell,m} C_{nst}^{k\ell m} \, _kq_\ell^m - \sum_{k,\ell,m} D_{nst}^{k\ell m} \, _kp_\ell^m = 0 \tag{77}$$

in which η_o is a reference viscosity value. The coefficients $A_{nst}^{k\ell m}$, $B_{nst}^{k\ell m}$, $C_{nst}^{k\ell m}$, and $D_{nst}^{k\ell m}$ which appear in these coupled equations involve a complicated combination of integrals of the viscosity coefficients (69) and the flow basis functions (73). Explicit, analytic expressions for these terms may be found in *Forte & Peltier* (1994).

Equation (76) describes the flow that is directly excited by buoyancy forces. We note that in a mantle with lateral viscosity variations, the *buoyancy forces directly excite a toroidal flow*. We observed in Lecture 1 that this is not possible with a viscosity that only varies with radius. The poloidal and toroidal flow components excited by buoyancy forces are not independent. Equation (77) describes the explicit coupling which must exist between poloidal and toroidal flow as a consequence of lateral viscosity variations. (This coupling was of course absent in a mantle with pure radial variations of viscosity – see Lecture 1.)

4.3. Generalized Green functions for flow with lateral viscosity variations

The coupled algebraic flow equations (76-77) may be written as the following simple matrix equations:

$$\mathbf{A}\,\mathbf{p} + \mathbf{B}\,\mathbf{q} = \mathbf{d} \tag{78}$$

$$\mathbf{C}\,\mathbf{q} = \mathbf{D}\,\mathbf{p} \tag{79}$$

in which the column vectors $\mathbf{p}$,$\mathbf{q}$ consist of the elements $_k p_\ell^m$ and $_k q_\ell^m$, respectively. The matrices $\mathbf{A}$, $\mathbf{B}$, $\mathbf{C}$, $\mathbf{D}$ are of course composed of the elements $A_{nst}^{k\ell m}$, $B_{nst}^{k\ell m}$, $C_{nst}^{k\ell m}$, and $D_{nst}^{k\ell m}$, respectively, in which the ordered triplet $(k\ell m)$ identifies the column position while the triplet (nst) identifies the row position in these matrices. The column vector $\mathbf{d}$ in (78) consists of the buoyancy term on the right hand side of equation of (76):

$$d_{nst} = \frac{2(\Omega_1^s)^2}{\eta_o} \int_b^a \frac{(\rho_1)_s^t(r)^*}{r} \, f_n(r) \, g_o(r) \, r^2 \, dr \tag{80}$$

A straightforward inversion of the matrix equations (78-79) yields the solution

for the flow coefficients in (73):

$$_k p_\ell^m = \sum_{n,s,t} P_{k\ell m}^{nst} \, d_{nst} \tag{81}$$

$$_k q_\ell^m = \sum_{n,s,t} Q_{k\ell m}^{nst} \, d_{nst} \tag{82}$$

in which $P_{k\ell m}^{nst}$ and $Q_{k\ell m}^{nst}$ are elements of the following matrices:

$$\mathbf{P} = \left[\mathbf{A} + \mathbf{B}\mathbf{C}^{-1}\mathbf{D}\right]^{-1} \tag{83}$$

$$\mathbf{Q} = \mathbf{C}^{-1}\mathbf{D}\mathbf{P} \tag{84}$$

Substitution of expressions (81-82) into the radial expansions (73), and using expression (80), we obtain the following explicit, analytic expressions for the

poloidal and toroidal flow solutions:

$$p_\ell^m(r) = \frac{g_o}{\eta_o} \int_b^a \sum_{s,t} \left[\sum_{k,n} f_k(r) P_{k\ell m}^{nst} f_n(r') 2(\Omega_1^s)^2 r'^2 \right] \frac{(\rho_1)_s^t(r')^*}{r'} \, dr' \qquad (85)$$

$$q_\ell^m(r) = \frac{g_o}{\eta_o} \int_b^a \sum_{s,t} \left[\sum_{k,n} g_k(r) Q_{k\ell m}^{nst} f_n(r') 2(\Omega_1^s)^2 r'^2 \right] \frac{(\rho_1)_s^t(r')^*}{r'} \, dr' \qquad (86)$$

Recall from Lecture 1 that the expression for the poloidal flow scalar in a mantle with a spherically symmetric viscosity distribution is given by:

$$p_\ell^m(r) = \frac{g_o}{\eta_o} \int_b^a p_\ell(r, r') \frac{(\rho_1)_\ell^m(r')}{r'} \, dr' \qquad (87)$$

in which $p_\ell(r, r')$ is the *poloidal-flow Green function*. If we compare expressions (85-86) with expression (87), we may immediately see that in a mantle with lateral viscosity variations the *generalized Green functions* for poloidal and

toroidal flows are:

$$P_{\ell m}^{st}(r, r') = \sum_{k,n} f_k(r) P_{k\ell m}^{nst} f_n(r') 2(\Omega_1^s)^2 r'^2 \tag{88}$$

$$Q_{\ell m}^{st}(r, r') = \sum_{k,n} g_k(r) Q_{k\ell m}^{nst} f_n(r') 2(\Omega_1^s)^2 r'^2 \tag{89}$$

The harmonic coefficient of the horizontal divergence of the surface flow is given by the following expression (see Lecture 1):

$$(\boldsymbol{\nabla}_{\mathbf{H}} \cdot \mathbf{u})_\ell^m (r = a) = \frac{\ell(\ell + 1)}{a} \left[\frac{d}{dr} p_\ell^m(r) \right]_{r=a}$$

If we now substitute the poloidal flow solution (85) into the above expression, we find:

$$(\boldsymbol{\nabla}_{\mathbf{H}} \cdot \mathbf{u})_\ell^m (r = a) = \frac{g_o}{\eta_o} \int_b^a \sum_{s,t} S_{\ell m}^{st}(r') \, (\rho_1)_s^t(r')^* \, dr' \tag{90}$$

in which we have the *generalized divergence kernel*:

$$S_{\ell m}^{st}(r') = \frac{\ell(\ell+1)}{a} \sum_{k,n} \left[\frac{df_k(r)}{dr}\right]_{r=a} P_{k\ell m}^{nst} f_n(r') 2(\Omega_1^s)^2 r' \qquad (91)$$

We may now compare expression (90) with the expressions (40-41) for the surface divergence generated by mantle flow which is coupled to rigid tectonic plates at the surface:

$$(\boldsymbol{\nabla}_{\mathrm{H}} \cdot \mathbf{u})_{\ell}^{m}(r=a) = \frac{\mathrm{g}_o}{\eta_o} \int_{b}^{a} \sum_{s,t} \left[\mathrm{P}_{\ell m,\,st}\, S_s(r')\right] \delta\rho_s^t(r')\, dr' \qquad (92)$$

We thus note that from the perspective of the predicted surface flow, lateral viscosity variations may also be regarded as generating a 'projection' of the internal density anomalies which is analogous to that of rigid surface plates. By virtue of expression (91) and the analogous form of expressions (90,92), we write this equivalent projection operator as:

$$\mathrm{P'}_{\ell m,\,st}(r') = S_{\ell m}^{st}(r') \left[S_s(r')\right]^{-1}$$

We have not yet specified the radial basis functions in expression (73). The only constraint is that the basis functions must satisfy the boundary conditions (50-52). If we simply assume *free-slip*, zero radial velocity conditions on the bounding surfaces $r = a, b$, then the poloidal and toroidal flow scalars must satisfy the conditions:

$$p_\ell^m(r) = \frac{d^2 p_\ell^m(r)}{dr^2} = \frac{d}{dr}\left(\frac{q_\ell^m(r)}{r}\right) = 0 \; , \;\; \text{at} \; r = a, b \qquad (93)$$

A very simple set of orthogonal radial basis functions which satisfy these boundary conditions are, for poloidal and toroidal flow respectively:

$$f_k(r) = \sin k\pi\left(\frac{r-a}{a-b}\right) \;\; \text{and} \;\; g_k(r) = r\cos k\pi\left(\frac{r-a}{a-b}\right) \qquad (94)$$

4.4. Application to a tomography-based flow calculation

To investigate the effects of lateral viscosity heterogeneity on mantle flow we shall express the spatial variations of viscosity as follows:

$$\eta(r, \theta, \phi) = \eta_o(r) \left[1 + \nu(r, \theta, \phi)\right] \tag{95}$$

in which $\eta_o(r)$ is the *horizontal average* of the 3-D viscosity function $\eta(r, \theta, \phi)$ at any radius r, and $\nu(r, \theta, \phi)$ describes the lateral variations in viscosity *relative to this average* (*i.e.,* the horizontal average of $\nu(r, \theta, \phi)$ is exactly zero at all radii).

The study of thermo-chemical heterogeneity in the lower mantle by *Forte & Mitrovica* (2001) led to an estimate of long-wavelength, lateral temperature variations, at the top the seismic D″-layer (*i.e.,* at 2740 km depth), shown below in Fig. 9.
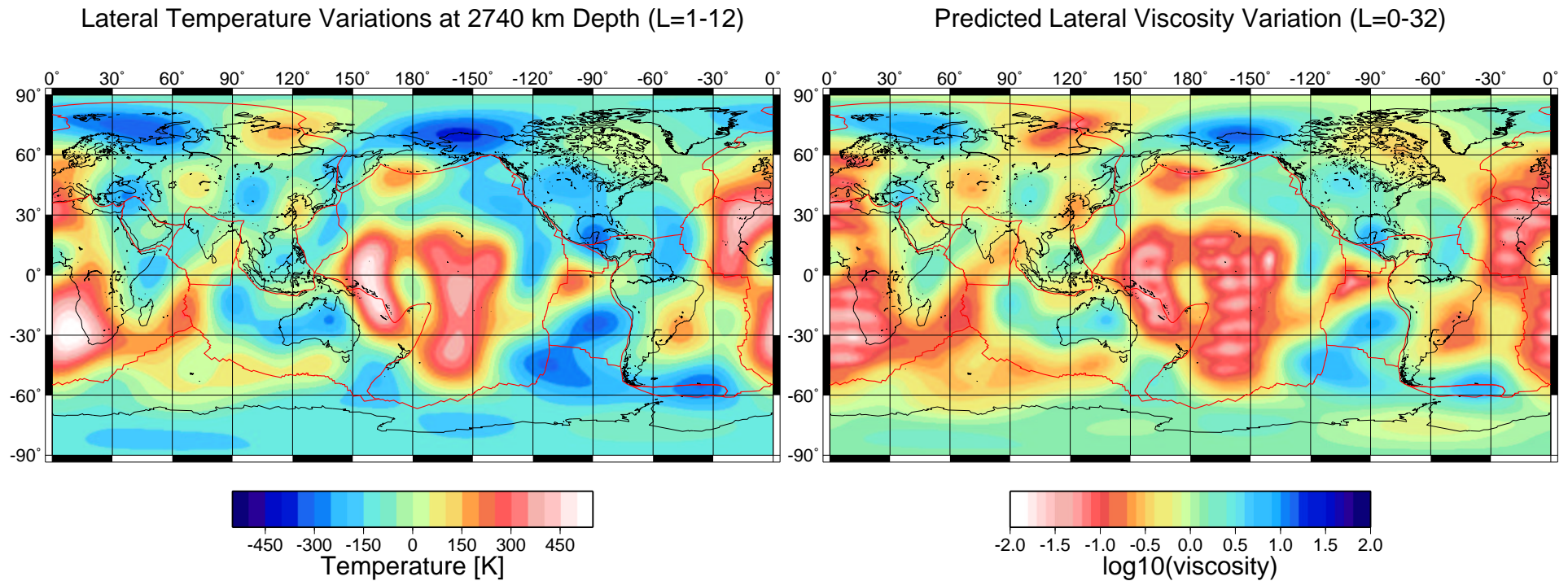
Fig. 9. Estimate (*left*) of lateral temperature variations obtained by *Forte & Mitrovica* (2001) on the basis of the long-wavelength tomography model of *Su & Dziewonski* (1997). On the *right* is the corresponding prediction of lateral viscosity variations (see main text for details).

The lateral viscosity variations which may be estimated on the basis of the tomography-derived temperature anomalies (Fig. 9) can be calculated on the basis of the homologous-temperature scaling in expression (2). We estimate an adiabatic temperature of $T_o = 2310K$ at 2740 km depth and we employ an estimated melting temperature of about $T_{melt} = 4260K$, derived from the study

of *Zerr et al.* (1998). The total temperature anomalies at a depth of 2740 km, $T(r, \theta, \phi) = T_o(r) + \delta T(r, \theta, \phi)$, are then obtained by adding the estimated lateral temperature anomalies in Fig. 9 to the mean adiabatic temperature.

In order to obtain a field of lateral viscosity variations which we could numerically resolve in the variational calculation of mantle flow, the empirical g factor in expression (2) was set to a value of 10. This value is significantly less than g values in the range of 20 to 30 estimated for olivine (*e.g., Weertman & Weertman*, 1975) but, as we noted in the Introduction, there is considerable uncertainty concerning the homologous temperature scaling in the lower mantle. *Karato & Karki* (2001) used $g = 10, 20$ in their investigation of the impact of seismic anelasticity in the lower mantle. The non-dimensional field of viscosity heterogeneity $1 + \nu(r, \theta, \phi)$, which we calculate using expression (2), is mapped out in Fig. 9 on a logarithmic scale. We observe from this figure that long-wavelength viscosity heterogeneity in the deep mantle can span at least 3 orders of magnitude.

We shall assume, for simplicity, that the large-amplitude, long-wavelength lateral viscosity variations in Fig. 9 extend across the entire mantle (*i.e.*, the

lateral viscosity variations are the same at all depths). We will also assume that mean (horizontally-averaged) viscosity increases smoothly with depth, according to the simple expression:

$$\eta_o(r) = \left(\frac{a}{r}\right)^n$$

where we choose $n = 10$, yielding a mean viscosity at the CMB which is 420 times greater than the viscosity at the top of the mantle. (There is no special significance in this number. We choose an n value sufficiently large so that the amplitude of the radial viscosity variation is of the same order of magnitude as the amplitude of the lateral viscosity variation.)

The buoyancy forces in the mantle will be derived from the *Su & Dziewonski* (1997) model of shear velocity heterogeneity, using the *Karato & Karki* (2001) velocity-to-density conversion profile shown in Lecture 1 (Fig. 14).

The mantle flow driven by these buoyancy forces, in the presence of the lateral viscosity variations shown in Fig. 9, is illustrated below in Fig. 10. For comparison we also show the purely divergent flow which is calculated in the absence of lateral viscosity variations.
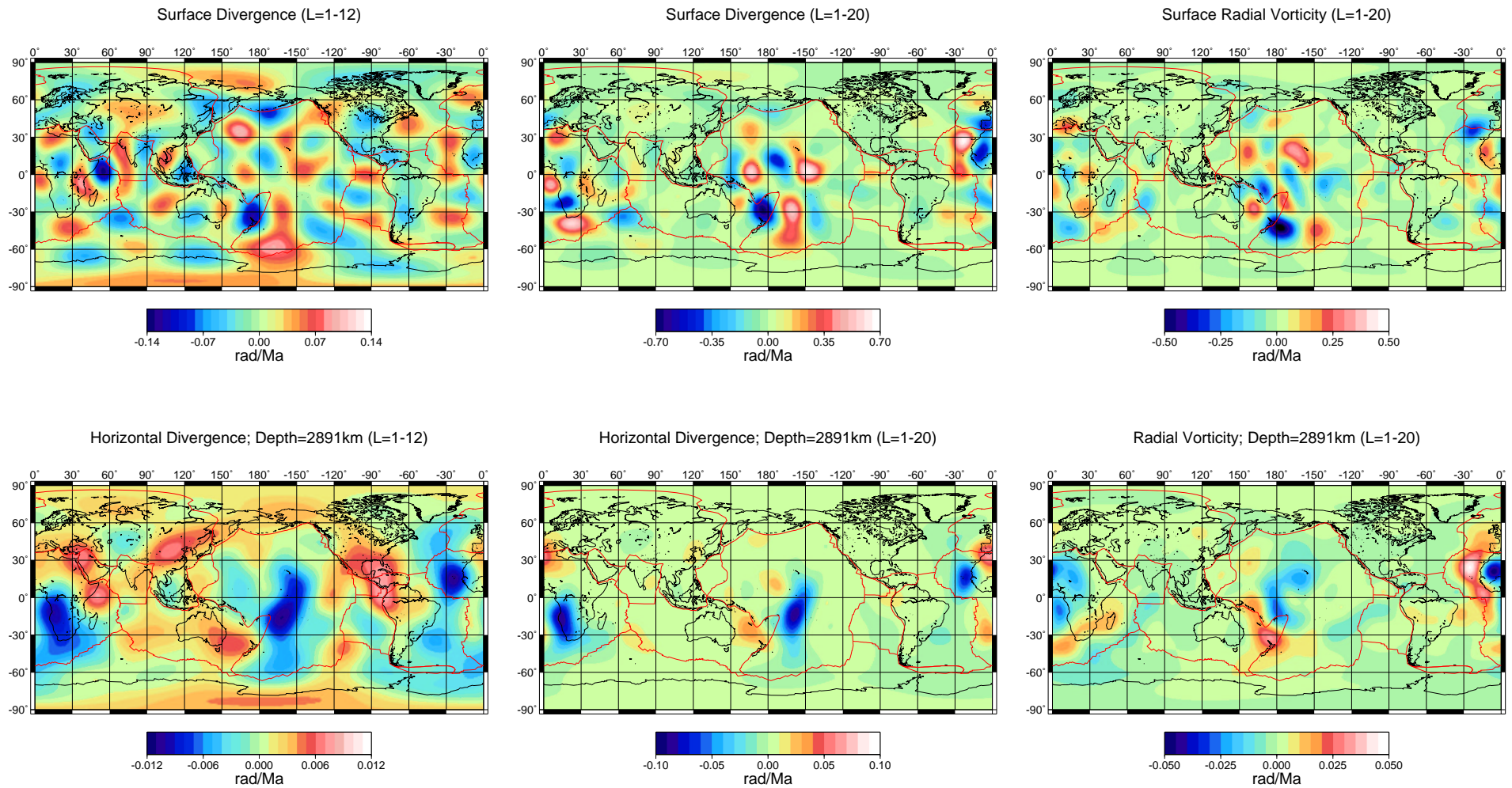
Fig. 10. (*top*) Surface flow predicted, in the left map, with pure radially varying viscosity, and with lateral viscosity variations in the two right maps (divergence and radial vorticity, respectively). (*bottom*) Flow predictions at the bottom of the mantle, at the core-mantle boundary.

We note in Fig. 10 that the strongly reduced viscosity below the central Pacific Ocean and below Africa (see Fig. 9) has resulted in a strong concentration of flow, with increased amplitude, below these regions. The flow below the continents, in the circum-Pacific region, has been strongly suppressed by the local increase of mantle viscosity. We also note that the amplitude of the radial vorticity field, which is dependent on the toroidal component of mantle flow (see Lecture 1), is comparable to the amplitude of the horizontal divergence field, which is a manifestation of the poloidal component of mantle flow. Evidently, the long-wavelength lateral viscosity variations in Fig. 9 are sufficiently strong to generate significant poloidal-toroidal coupling at all depths in the mantle.

The impact of the lateral viscosity variations on less direct manifestations of the mantle flow, such as dynamic topography, is illustrated in Fig. 11 where we show the predicted deflections of the CMB. A detailed presentation on the theoretical calculation of dynamic surface topography, in the presence of lateral viscosity variations, may be found in *Forte & Peltier* (1994). We note here, in strong contrast to the flow predictions (Fig. 10), that the effect of lateral viscosity variations on flow-induced surface topography is strongly muted. The relative root-mean-square difference between the two predictions in Fig. 11 is only 25%.

This is more than an order of magnitude less than the effect on the flow field shown in Fig. 10. As explained in *Forte & Peltier* (1994), the relative insensitivity of dynamic topography, and hence the geoid anomalies, on lateral viscosity variations is due to the 'internal cancellation' of the viscosity heterogeneity when calculating the dynamic stress field.
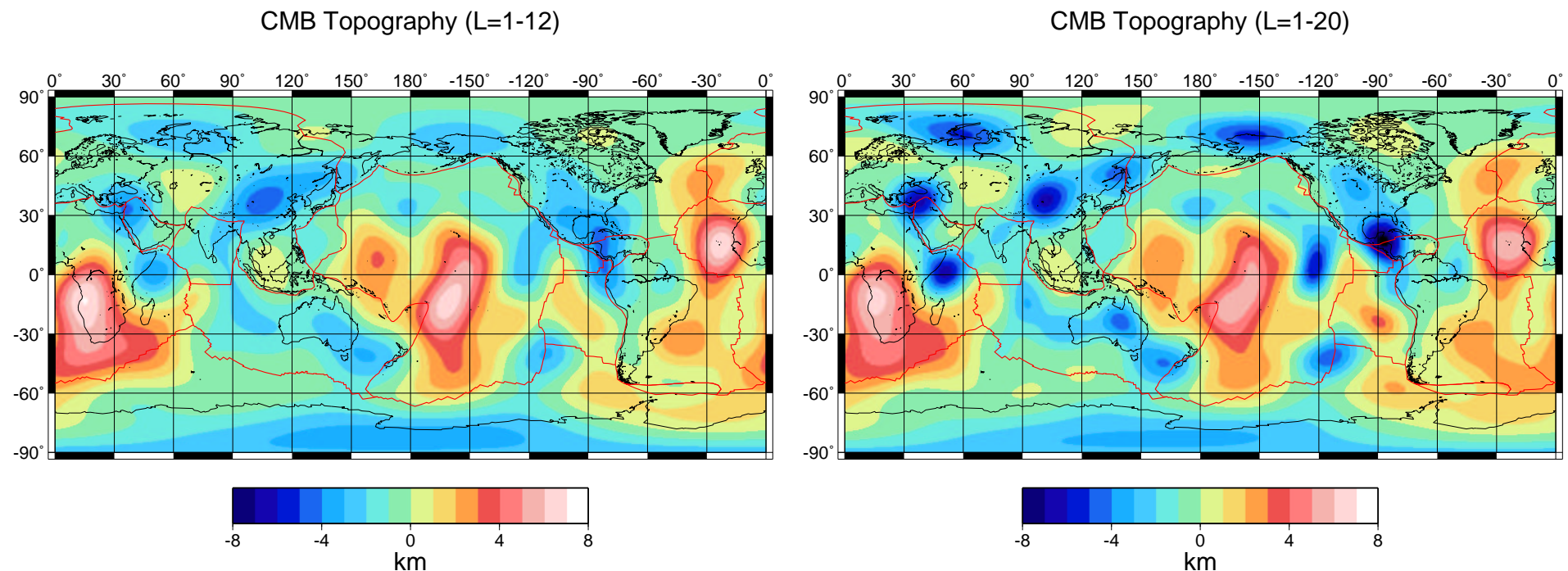

Fig. 11. (*left*) Flow-induced CMB topography predicted with pure radial variations in viscosity and, (*right*) predicted with superimposed lateral viscosity variations.

5. References

- Aki, K., and P.G. Richards, *Quantitative Seismology*, Vol. II, W.H. Freeman (San Francisco, USA), 1980.

- Backus, G, A class of self-sustaining dissipative spherical dynamos, *Ann. Phys.*, **4**, 372–447, 1958.

- Batchelor, G.K., *An Introduction to Fluid Dynamics*, Cambridge University Press (Cambridge, UK), 1967.

- Borch, R.S., and H.W. Green, Dependence of creep in olivine on homologous temperature and its implications for flow in the mantle, *Nature*, **330**, 345–348, 1987.

- Brown, J.M., Mantle melting at high pressure, *Science*, **262**, 529–530, 1993.

- Čadek, O., Y. Ricard, Z. Martinec, and C. Matyska, Comparison between Newtonian and non-Newtonian flow driven by internal loads, *Geophys. J. Int.*, **112**, 103-114, 1993.

- Carter, N.L., Steady state flow of rocks, *Rev. Geophys. Space Phys.*, **14**, 301–360, 1976.

- Christensen, U., Convection with pressure- and temperature-dependent non-Newtonian rheology, *Geophys. J. R. Astron. Soc.*, **77**, 343–384, 1984.

- Christensen, U., and H. Harder, 3-D convection with variable viscosity, *Geophys. J. Int.*, **104**, 213-226, 1991.

- Constable, S.C., R.L. Parker, and C.G. Constable, Occam's inversion: A practical algorithm for generating smooth models from electromagnetic sounding data, *Geophys.*, **52**, 289–300, 1987.

- De Mets, C.R., R.G. Gordon, D.F. Argus, and S. Stein, Current plate motions, *Geophys. J. Int.*, **101**,

425–478, 1990.

- Edmonds, A.R., *Angular Momentum in Quantum Mechanics*, Princeton University Press (Princeton, New Jersey, USA), 1960.

- Forte, A.M., The kinematics and dynamics of poloidal-toroidal coupling of mantle-flow, *Eos Trans. AGU*, **73**, 273, Spring Meeting Suppl., 1992.

- Forte, A.M., and J.X. Mitrovica, Deep-mantle high-viscosity flow and thermochemical structure inferred from seismic and geodynamic data, *Nature*, **410**, 1049–1056, 2001.

- Forte, A.M., and W.R. Peltier, Viscous flow models of global geophysical observables,1 Forward problems *J. Geophys. Res.*, **96**, 20,131–20,159, 1991.

- Forte, A.M., and W.R. Peltier, The kinematics and dynamics of poloidal-toroidal coupling in mantle flow: The importance of surface plates and lateral viscosity variations, *Advances in Geophysics*, **36**, 1–119, 1994.

- Gable, C.W., R.J. O'Connell, and B.J. Travis, Convection in three dimensions with surface plates, *J. Geophys. Res.*, **96**, 8391–8405, 1991.

- Goldstein, H., *Classical Mechanics*, 2nd ed., Addison-Wesley (Reading, Massachusetts, USA), 1980.

- Gordon, R.B., Diffusion creep in the earth's mantle, *J. Geophys. Res.*, **70**, 2413–2418, 1965.

- Grand, S.P., Mantle shear-wave tomography and the fate of subducted slabs, *Phil. Trans. R. Soc. Lond. A*, **360**, 2475–2491, 2002.

- Hager, B.H., and R.J. O'Connell, A simple global model of plate dynamics and mantle convection, *J.*

Geophys. Res., **86**, 4843–4867, 1981.

- Hirth, G., and D. Kohlstedt, Rheology of the upper mantle and the mantle wedge: A view from the experimentalists, in *Inside the Subduction Factory*, edited by J. Eiler, AGU Geophysical Monograph 138, pp. 83–105, American Geophysical Union (Washington, DC, USA), 2003.

- Justice, J.H., Two-dimensional recursive filtering in theory and practice, in *Applied Time Series Analysis*, edited by D.F. Findley, Academic Press (New York, USA), 1978.

- Karato, S., and B.B. Karki, Origin of lateral variation of seismic wave velocities and density in the deep mantle, *J. Geophys. Res.*, **106**, 21,771–21,784, 2001.

- Karato, S.-I., M.S. Paterson, J.D. Fitzgerald, Rheology of synthetic olivine aggregates: Influence of grain size and water, *J. Geophys. Res.*, **91**, 8151–8176, 1986.

- Lanczos, C., *Linear Differential Operators*, Van Nostrand (New York, USA), 1961.

- Mitrovica, J.X., and A.M. Forte, A new inference of mantle viscosity based upon joint inversion of convection and glacial isostatic adjustment data, *Earth Planet. Sci. Lett.*, *in press*, 2004.

- Nicolas, A., and J.-P. Poirier, *Crystalline Plasticity and Solid State Flow in Metamorphic Rocks*, John Wiley (New York, USA), 1976.

- Phinney, R.A., and R. Burridge, Representation of the elastic-gravitational excitation of a spherical Earth model by generalized spherical harmonics, *Geophys. J. R. Astron. Soc.*, **34**, 451–487, 1973.

- Post, R.L. Jr., and D.T. Griggs, The Earth's mantle: evidence of non-Newtonian flow, *Science*, **181**, 1242–1244, 1973.

- Ribe, N.M., The dynamics of thin-shells with variable viscosity and the origin of toroidal flow, *Geophys. J. Int.*, **110**, 537–552, 1992.

- Ricard, Y., and C. Vigny, Mantle dynamics with induced plate tectonics, *J. Geophys. Res.*, **94**, 17543–17559, 1989.

- Ricard, Y., M. Richards, C. Lithgow-Bertelloni, and Y. Le Stunff, A geodynamic model of mantle density heterogeneity, *J. Geophys. Res.*, **98**, 21,895–21,909, 1993.

- Richards, M.A., and D.C. Engebretson, Large-scale mantle convection and the history of subduction, *Nature*, **355**, 437–440, 1992.

- Ricoult, D.L., and D.L. Kohlstedt, Experimental evidence for the effect of chemical environment upon the creep rate of olivine, in *AGU Geophys. Monogr. Ser.*, vol. 31, pp. 171–184, American Geophysical Union (Washington, DC, USA), 1985.

- Stocker, R.L., and M.F. Ashby, On the rheology of the upper mantle, *Rev. Geophys. Space Phys.*, **11**, 391–426, 1973.

- Su, W., and A.M. Dziewonski, Simultaneous inversion for 3-D variations in shear and bulk velocity in the mantle, *Phys. Earth Planet. Inter.*, **100**, 135–156, 1997.

- Weertman, J., The creep strength of the earth s mantle, *Rev. Geophys. Space Phys.*, **8**, 145–168, 1970.

- Weertman, J., Creep laws for the mantle of the Earth, *Philos. Trans. R. Soc. London, Ser. A.*, **288**, 9–26, 1978.

- Weertman, J., and J.R. Weertman, High temperature creep of rock and mantle viscosity, *Annu. Rev. Earth Planet. Sci.*, **3**, 293–315, 1975.

- Zerr, A., A. Diegler, and R. Boehler, Solidus of Earth's deep mantle, *Science*, **281**, 243–246, 1998.

- Zhang, S., and U. Christensen, Some effects of lateral viscosity variations on geoid and surface velocities induced by density anomalies in the mantle, *Geophys. J. Int.*, **114**, 531-547, 1993.

- Zhong, S., M. Gurnis, and L. Moresi, The role of faults, nonlinear rheology, and viscosity structure in generating plates from instantaneous mantle flow models. *J. Geophys. Res.*, **103**, 15,255–15,268, 1998.